Published in final edited form as:
Sci Immunol. 2024 April 12; 9(94): eadn1452. doi:10.1126/sciimmunol.adn1452.

The palmitoylation of gasdermin D directs its membrane translocation and pore formation during pyroptosis

Arumugam Balasubramanian[1], **Alan Y. Hsu**[1], **Laxman Ghimire**[1], **Muhammad Tahir**[1,8], **Pascal Devant**[2], **Pietro Fontana**[3], **Gang Du**[3], **Xing Liu**[4], **Dang Fabin**[5], **Hiroto Kambara**[1], **Xuemei Xie**[1], **Fei Liu**[1], **Tomoya Hasegawa**[1], **Rong Xu**[1], **Hongbo Yu**[6], **Wenyi Wei**[4], **Mei Chen**[7], **Steven Kolakowski**[7], **Sunia Trauger**[7], **Martin Røssel Larsen**[8], **Wenyi Wei**[5], **Hao Wu**[3], **Jonathan C. Kagan**[2], **Judy Lieberman**[4], **Hongbo R. Luo**[1,*]

[1]Department of Pathology, Dana-Farber/Harvard Cancer Center, Harvard Medical School; Department of Laboratory Medicine, Boston Children's Hospital; Enders Research Building, Room 811, Boston, MA, 02115, USA

[2]Division of Gastroenterology, Boston Children's Hospital and Harvard Medical School; 300 Longwood Avenue, Boston, MA 02115, USA

[3]Department of Biological Chemistry and Molecular Pharmacology, Harvard Medical School; Program in Cellular and Molecular Medicine, Boston Children's Hospital, Boston MA, USA

[4]Department of Pediatrics, Harvard Medical School; Program in Cellular and Molecular Medicine; Boston Children's Hospital, Boston, MA 02115, USA.

[5]Department of Pathology, Beth Israel Deaconess Medical Center, Harvard Medical School; Boston, MA, USA

[6]VA Boston Healthcare System, Department of Pathology and Laboratory Medicine; 1400 VFW Parkway, West Roxbury, MA 02132 USA

[7]Harvard Center for Mass Spectrometry, Harvard University; Boston, MA 02115, USA

[8]Biomedical Mass Spectrometry and Systems Biology, University of Southern Denmark; Odense, DK

[*]Corresponding author. Hongbo.luo@childrens.havard.edu.

Author contributions: Conceptualization: H.R.L. and A.B. Methodology: H.R.L., A.B., A.H., F.L., L.G., M.T., H.K., X.X., D.F., C.M., S.K., S.T., M.R.L., and H.Y. Investigation: A.B., A.H., L.G., C.M., S.K., P.F., G.D., H.W., S.T., M.R.L., F.L., and T.H. Resources: H.R.L., H.W., J.L., P.D., J.C.K., X.L., M.R.L., and W.W. Funding acquisition: H.R.L. Supervision: H.R.L. Writing: H.R.L. and A.B.

Competing interests: J.C.K. consults and holds equity in Corner Therapeutics, Larkspur Biosciences, MindImmune Therapeutics, and Neumora Therapeutics. H.W. is a cofounder of Ventus Therapeutics. All other authors declare no competing financial interests.

Supplementary Materials

This PDF file includes:
Figs. S1 to S13
Tables S1 to S4
Captions for Data S1 to S4
Reference (67)

Other Supplementary Material for this manuscript includes the following:
Data S1 to S4
MDAR Reproducibility Checklist

Abstract

Plasma membrane perforation elicited by caspase cleavage of the gasdermin D (GSDMD) N-terminal domain (GSDMD-NT) triggers pyroptosis. The mechanisms underlying GSDMD membrane translocation and pore formation are not fully understood. Here, using a proteomics approach, we identified fatty acid synthase (FASN) as a GSDMD-binding partner. S-palmitoylation of GSDMD at Cys191/192 (human/mouse), catalyzed by palmitoyl acyltransferases ZDHHC5 and ZDHHC9 and facilitated by reactive oxygen species (ROS), directly mediated membrane translocation of GSDMD-NT but not full-length GSDMD (GSDMD-FL). Palmitoylation of GSDMD-FL could be induced before inflammasome activation by stimuli such as lipopolysaccharide (LPS), consequently serving as an essential molecular event in macrophage priming. Inhibition of GSDMD palmitoylation suppressed macrophage pyroptosis and IL-1β release, mitigated organ damage, and enhanced the survival of septic mice. Thus, GSDMD-NT palmitoylation is a key regulatory mechanism controlling GSDMD membrane localization and activation, which may offer an additional target for modulating immune activity in infectious and inflammatory diseases.

One-sentence summary:

Palmitoylation of GSDMD at Cys191/Cys192 is required for its membrane translocation and pore-forming activity in macrophages.

INTRODUCTION

Pyroptosis is a form of lytic cell death triggered by proinflammatory signals, which plays a critical role in inflammation and host defense responses (1, 2). The pore-forming protein gasdermin D (GSDMD) is an executor of this process (3–6). Upon activation of the inflammasome, caspase-1 cleaves GSDMD into a GSDMD N-terminal pore-forming domain and a C-terminal autoinhibitory domain (3, 7). The cleaved N-terminal domain (GSDMD-NT) binds to phosphatidylinositol phosphates and phosphatidylserine in the cell membrane inner leaflet to form large oligomers, which generate approximately 20-nm pores in the plasma membrane and consequent lytic cell death (3, 5, 8–15). GSDMD can also be cleaved and activated by lipopolysaccharide (LPS)–induced activation of non-canonical inflammasomes via murine caspase-11 or human caspase-4 and −5. Additionally, caspase-8, neutrophil elastase (ELANE), and cathepsin G cleave GSDMD to induce lytic cell death in certain contexts (16–20). GSDMD-NT–mediated plasma membrane perforation triggers profound membrane rupture and subsequent lytic death to ultimately facilitate clearance of intracellular pathogens and the maturation and release of proinflammatory cytokines such as interleukin (IL)-1β and IL-18 (3–5, 15, 21). Moreover, GSDMD may also play an essential role in inflammasome-mediated IL-1β secretion from living macrophages (21).

GSDMD cleavage and GSDMD-mediated lytic cell death are tightly regulated. For instance, succination of GSDMD Cys191/Cys192 (human/mouse) prevents GSDMD–caspase interactions, limiting GSDMD processing, oligomerization, and its ability to induce cell death (22). The Ragulator–Rag–mTORC1 pathway promotes GSDMD oligomerization but not its membrane localization by mediating reactive oxygen species (ROS) production.

This provides a checkpoint for pore formation and consequent pyroptosis and uncouples biochemical GSDMD cleavage from pore formation (23). Oligomerization of GSDMD-NT at the plasma membrane produces a specialized plasma membrane pore structure that preferentially releases mature IL-1β and non-selective ionic fluxes (15). Oncotic cell swelling then ruptures the plasma membrane, which is not simply a passive event mediated by osmotic lysis but tightly regulated by cell surface NINJ1 protein during lytic pyroptotic cell death (24–26). GSDMD pores appear to be dynamic structures, with pore-mediated calcium influx modulating pore-opening and -closing kinetics through phosphoinositide metabolism (27). However, whether GSDMD plasma membrane translocation is tightly controlled and how this process is regulated remain elusive.

Here, we report that S-palmitoylation at Cys191/Cys192 of GSDMD is a key mechanism leading to its activation in pyroptosis. This process is crucial for anchoring the GSDMD-NT to the plasma membrane, thereby facilitating the rupture of the plasma membrane and subsequent pyroptotic cell death. This finding represents a significant advance in our understanding of the checkpoints involved in pyroptosis.

RESULTS

GSDMD interacts with fatty acid synthase (FASN) and undergoes palmitoylation

To further elucidate the physiological mechanisms controlling GSDMD processing and activation, we performed a proteomics analysis to identify GSDMD-interacting proteins. We expressed full-length GSDMD (GSDMD-FL) in HEK293T cells and immunoprecipitated GSDMD-containing protein complexes using a specific antibody targeting GSDMD (Fig. 1A). Coimmunoprecipitated proteins were eluted and analyzed by liquid chromatography–tandem mass spectrometry (LC–MS/MS) (data S1). Proteomics analysis identified fatty acid synthase (FASN) as a GSDMD-interacting protein (table S1). Immunoblotting confirmed endogenous FASN expression in HEK293T cells and its coimmunoprecipitation with recombinant GSDMD (Fig. 1B). To investigate whether GSDMD and FASN interact under pathophysiological conditions, phorbol 12-myristate 13-acetate (PMA)–differentiated macrophage-like THP-1 cells were treated with or without LPS. Coimmunoprecipitation analysis revealed that FASN interacted with endogenous GSDMD only in the presence of LPS (Fig. 1C). However, a protein pull-down assay revealed a direct interaction between the purified recombinant FASN and GSDMD proteins (Fig. 1D). The lack of interaction in unstimulated macrophages suggests that an inhibitory mechanism may prevent this interaction.

FASN catalyzes palmitate biosynthesis and is thus required for protein palmitoylation (28–31). There is growing evidence that interactions between FASN and palmitoylation targets are necessary for this protein modification (31–33). Our observation of a FASN–GSDMD interaction prompted us to examine therefore whether GSDMD can be palmitoylated. We transiently transfected HEK293T cells with a GSDMD-FL construct and assessed palmitoylated GSDMD levels after 24 hours using an acyl–biotin exchange (ABE) assay (Fig. 1E). Indeed, recombinant GSDMD was robustly palmitoylated in HEK293T cells, and pretreatment with hydroxylamine (HAM), which cleaves the thioester bond to generate a sulfhydryl group, was essential for detecting signal (Fig. 1F). Silencing FASN with a

specific *FASN* siRNA but not control scrambled siRNA significantly reduced GSDMD palmitoylation (Fig. 1G). Thus, GSDMD and FASN interact and FASN is required for GSDMD palmitoylation.

To identify which GSDMD region was palmitoylated, we transiently transfected HEK293T cells with GSDMD-FL, GSDMD-NT, and GSDMD-C terminal fragment (GSDMD-CT). Immunoblot analysis confirmed that both GSDMD-FL and GSDMD-NT but not GSDMD-CT were palmitoylated (Fig. 1H). Signals were significantly attenuated when cells were pretreated with the palmitate analog 2-bromopalmitate (2BP), an electrophilic α-brominated fatty acid widely used to inhibit protein palmitoylation (Fig. 1H). GSDMD palmitoylation appeared to be a general cellular event. It was also observed in doxycycline (Dox)–inducible mouse immortalized bone marrow–derived macrophages (iBMDMs) expressing GSDMD-NT (23) (fig. S1). We next examined palmitoylation of endogenous GSDMD in PMA-differentiated THP-1 cells. Prior to LPS stimulation, GSDMD palmitoylation was almost undetectable and was only observed in LPS/Nig-treated cells (Fig. 1I). Silencing FASN via treatment with a specific FASN siRNA, significantly reduced GSDMD palmitoylation (fig. S2). Similar to our observations in HEK293T cells, both full-length and cleaved N-terminal GSDMD in THP-1 cells were palmitoylated and 2BP inhibited palmitoylation (Fig. 1I). Palmitoylation of full-length and cleaved N-terminal GSDMD was also detected in mouse bone marrow-derived macrophages (mBMDMs), but only upon LPS/Nig stimulation (Fig. 1J). We examined the palmitoylation of several other well-known pore-forming proteins. In line with other reports (34, 35), we observed palmitoylation of GSDME. However, we did not detect any LPS-induced palmitoylation of MLKL (fig. S3, A and B).

GSDMD palmitoylation is critical for macrophage pyroptosis

To determine whether protein palmitoylation modulates pyroptosis, we treated PMA-differentiated macrophage-like THP-1 cells with 2BP or cerulenin, a FASN inhibitor (36–38). Inhibition of palmitoylation with cerulenin or 2BP significantly suppressed LPS/Nig-induced pyroptosis as measured by using SYTOX Green (Fig. 2, A and B). Similar results were observed when pyroptosis was assessed using a lactate dehydrogenase (LDH) cytotoxicity assay (Fig. 2C) or a luminescence-based cell viability assay to quantify the reducing potential as a surrogate of metabolically active cells (Fig. 2D). Consistently, the two inhibitors significantly suppressed cell death-associated IL-1β release (Fig. 2E). The depalmitoylation inhibitor palmostatin B (PMB) did not affect cell death (Fig. 2, A to E), suggesting that depalmitoylation may not be a prominent regulator of macrophage pyroptosis. Cerulenin can alter expression of NLRP3, IL-1β, and FASN in macrophages (39). Indeed, it significantly suppressed caspase-1 activity in THP-1 cells, suggesting that its effect on macrophage pyroptosis may not be a direct consequence of GSDMD palmitoylation (Fig. 2F). We consequently used 2BP exclusively in all subsequent experiments as a more specific palmitoylation inhibitor as it did not affect caspase-1 activity (Fig. 2F) and GSDMD cleavage (fig. S4, A and B) but inhibited LPS/Nig-induced cell death in a dose-dependent manner (Fig. 2, G to I). As a general inhibitor of palmitoylation, 2BP targets multiple proteins including NLRP3 (40) and MyD88 (31), but it did not affect NLRP3 expression in macrophages (fig. S4, C to E).

Both SYTOX Green uptake (Fig. 2, J and K) and LDH release (Fig. 2L) assays confirmed that inhibition of protein palmitoylation by 2BP also suppressed LPS/Nig-induced cell death in primary mBMDMs. As expected, LPS/Nig-induced pyroptosis was also drastically reduced in *Gsdmd*-deficient mBMDMs. However, 2BP did not further inhibit the death of *Gsdmd*-deficient mBMDMs, suggesting that its effect was specific for GSDMD-mediated cell death (Fig. 2, J to L).

To further confirm that the effect of GSDMD palmitoylation on cell death is directly mediated by the cytotoxic, pore-forming activity of GSDMD-NT, HEK293T cells expressing GSDMD-NT were treated with 2BP, and GSDMD-NT-induced cell death was measured by propidium iodide (PI) uptake and LDH release. 2BP treatment significantly reduced GSDMD-NT-induced lytic cell death in both assays (fig. S5, A and B) without affecting GSDMD-NT expression (fig. S5C). Next, we established an inducible system in which recombinant human GSDMD-NT protein was expressed in a doxycycline (Dox)-inducible manner in HAP1 cells constitutively expressing EGFP. GSDMD-NT–mediated cell death was assessed by measuring GFP fluorescence intensity, PI staining (fig. S5, D and E), LDH release (fig. S5F), and cellular reducing potential (fig. S5G). Dox-induced GSDMD-NT expression induced prominent cell death according to all four metrics. Treatment with palmitoylation inhibitors rescued cells from pyroptotic cell death. In this inducible system, palmitoylation inhibitors did not alter GSDMD-NT expression, with similar amounts of recombinant protein expressed in untreated and inhibited cells (fig. S5H). Moreover, the inhibition of palmitoylation had no effect on Dox-induced GFP expression, again suggesting that palmitoylation did not alter transcription or translation (fig. S5I). Finally, 2BP-induced inhibition of pyroptosis was also observed in iBMDMs expressing GSDMD-NT (fig. S1, C to E). Thus, palmitoylation is required for GSDMD-mediated pyroptosis, likely by facilitating GSDMD-NT activation.

GSDMD palmitoylation occurs on Cys192

Palmitoylation often occurs on cysteine residues and, less frequently, on serine and threonine residues. To map the palmitoylation site in GSDMD-NT, we mutated each cysteine in GSDMD-NT (Fig. 3A). GSDMD-NT palmitoylation only significantly decreased when Cys192 but not other cysteine residues was mutated (Fig. 3B). Cells transfected with mutant GSDMD-NT were examined for LDH release. Wild-type (WT) GSDMD-NT induced LDH release, whereas Cys192A, but not other mutations, significantly decreased LDH release (Fig. 3C). Similar results were observed in iBMDMs expressing GSDMD-NT (fig. S1, A to E). Additionally, the effect of 2BP on cell death was abolished when Cys192 was mutated (fig. S1, A to E). Next, we confirmed using mass spectrometry that the palmitoylation primarily occurred on Cys191/192 of GSDMD (Fig. 3, D to F and data S2). The palmitoylation was exclusively detected on Cys191/192 and not on other cysteine residues. Consistent with previous work (41), we did not observe oxidation on Cys191/192 in the absence of inflammasome activation (Fig. 3E).

To definitively confirm Cys191/192 was palmitoylated, we treated cells with an alkyne-tagged palmitic acid analogue and subsequently labeled palmitoylated protein via a click-chemistry conjugate (42) (fig. S6A). Palmitoylated GSDMD-NT levels were higher in WT

and Cys39, Cys57, Cys77, Cys122, and Cys265 mutants, but the palmitoylation signal was much weaker in the Cys192 mutant (fig. S6B). As expected, HAM could cleave the thioester bond and remove the palmitoyl moiety from the protein. Similarly, palmitoylation was also significantly suppressed when Cys192 was mutated in the GSDMD-FL (fig. S6C).

GSDMD Cys191/Cys192 can also be succinated (22). When the levels of GSDMD succination increased, there was a corresponding decrease in GSDMD palmitoylation (fig. S6D). Thus, GSDMD succination can negatively regulate GSDMD palmitoylation during pyroptotic cell death.

After pinpointing the palmitoylation site of GSDMD, we developed a strategy to selectively inhibit its palmitoylation. We designed a competitive peptide corresponding to the conserved GSDMD palmitoylation region (Fig. 3G), an approach commonly applied for target-specific palmitoylation inhibition (43–47). A cell-permeable peptide (CPP), CPP-R9 (polyarginine), was fused to the GSDMD peptide (CPP-W) to achieve delivery to the cytosol of target cells. A peptide carrying a C192A substitution (CPP-M) was synthesized and used as a negative control (Fig. 3H). CPP-W, but not CPP-M, efficiently suppressed GSDMD palmitoylation (fig. S7A) and consequently inhibited the death of Dox-inducible HAP1 cells expressing GSDMD-NT, as measured by GFP expression and PI staining (fig. S7B), LDH release (fig. S7C), and cellular reducing potential (fig. S7D). Similar pyroptosis-blocking effects were detected in mBMDMs challenged with LPS/Nig (fig. S7, E to H), THP-1 cells challenged with LPS/Nig (Fig. 3, I to M), as well as iBMDMs expressing GSDMD-NT (fig. S1, A to E). CPP-W demonstrated no impact on other palmitoylation targets such as NLRP3 (40) and MyD88 (31), highlighting its specificity (fig. S3, A and B). In addition, NLRP3 expression was unaltered in CPP-W treated cells (fig. S3A). When cells were exposed to 2BP, the protective effects conferred by CPP-W were nullified (Fig. 3, I to M), thereby confirming that the observed effects were mediated by protein palmitoylation.

GSDMD palmitoylation directs membrane translocation of GSDMD-NT but not GSDMD-FL

GSDMD cleavage was independent of its palmitoylation, and inhibiting GSDMD palmitoylation with 2BP did not impact cleavage (Fig. 1, I and J). Furthermore, inhibition of GSDMD palmitoylation did not affect the interaction between the GSDMD C-terminal and N-terminal fragments (fig. S8A). Thus, palmitoylation appears to play a role in processes other than GSDMD cleavage and autoinhibition.

Palmitate acts as a hydrophobic membrane anchor, stably attaching palmitoylated protein to the cellular membrane. Consistently, S-palmitoylation significantly enhanced the binding of GSDMD-NT to phosphatidylinositol phosphate and cardiolipin, but not phosphatidylcholine (Fig. 4, A and B). Thus, although the specificity of lipid binding is likely determined by GSDMD-NT protein structure, S-palmitoylation significantly enhances its binding. Notably, full-length GSDMD demonstrated no binding to lipids, even after palmitoylation (Fig. 4, A and B).

Next, we examined whether GSDMD-NT palmitoylation was required for its membrane localization in cells. HEK293T cells were transiently transfected with WT or Cys192A-mutant GSDMD-NT and then treated with or without 2BP. GSDMD-NT localization was

determined by both immunofluorescence imaging (Fig. 4C) and subcellular fractionation (Fig. 4D). Consistent with previous studies (10, 18), GSDMD-NT was predominantly membrane localized whereas GSDMD-NT-Cys192A was cytosolic. However, WT GSDMD-NT relocated to the cytoplasm upon 2BP treatment (Fig. 4, C and D). Similar results were observed when recombinant human GSDMD-NT protein was expressed in a Dox-inducible manner in HAP1 cells (Fig. 4E). Although GSDMD-FL could be palmitoylated, its location remained cytosolic in HEK293 cells (fig. S8B) as well as in both unstimulated and LPS-stimulated THP-1 cells (fig. S8C). Thus, palmitoylation specifically governs the membrane translocation of cleaved GSDMD-NT. In the GSDMD-FL, the palmitoyl group may be nestled within a hydrophobic pocket, preventing it from being readily accessible for membrane binding (46, 48–50).

Next, we investigated the effect of palmitoylation on GSDMD-NT oligomerization using native PAGE gel electrophoresis (10, 22, 23). WT GSDMD-NT, but not the Cys192 mutant, formed oligomers. 2BP or CPP-W could both significantly reduce this oligomerization (Fig. 4F). suggesting that palmitoylation of GSDMD mediated both its membrane translocation and oligomerization. Thus, S-palmitoylation is an important factor controlling GSDMD-NT localization and pore formation in pyroptosis.

ZDHHC5 and ZDHHC9 palmitoylate GSDMD

Palmitoylation is mediated by palmitoyl acyl transferase (PAT) enzymes, a family of zinc finger and DHHC motif-containing (ZDHHC) proteins that transfer palmitate onto the thiol group of cysteine from cytosolic palmitoyl-CoA. Acyl protein thioesterases (APTs; depalmitoylation enzymes) can reverse this process (51) (fig. S9A). Twenty-four human DHHC domain proteins have been identified to date: 17 are known to have PAT activity (51). ZDHHC proteins have distinct substrate specificities. To discern the specific palmitoyl acyl transferases responsible for GSDMD palmitoylation and pyroptosis, we first identified which ZDHHC proteins were expressed in HEK293T cells. *ZDHHC1, ZDHHC8, ZDHHC11, ZDHHC15, ZDHHC19,* and *ZDHHC22* mRNAs were almost undetectable by RT-qPCR in HEK293T cells (fig. S9B). We then co-transfected HEK293T cells with GSDMD-NT and siRNAs targeting each ZDHHC with PAT activity expressed in these cells, screening for siRNAs that suppressed GSDMD-NT-induced pyroptotic death as measured by an LDH release assay. ZDHHC5 and ZDHHC9 were the most potent mediators of GSDMD palmitoylation (fig. S9C). We performed a similar screening in HAP1 cells expressing recombinant human GSDMD-NT protein in a Dox-inducible manner. Again, siRNAs targeting *ZDHHC5* and *ZDHHC9* most potently decreased LDH release compared with scrambled control siRNA (fig. S9D). The ABE assay revealed that silencing *ZDHHC5* or/and *ZDHHC9* significantly reduced GSDMD-NT palmitoylation compared with cells transfected with control scrambled siRNA (fig. S9, E to G). Both ZDHHC5 and 9 were required for maximum LDH release, further demonstrating that GSDMD needs both palmitoyl enzymes to induce pyroptosis (fig. S9H). Additionally, fluorescent imaging showed that GSDMD-NT-induced PI uptake was inhibited when either *ZDHHC5* or *ZDHHC9* was knocked down (fig. S9I). By contrast, knocking down another *ZDHHC* protein, *ZDHHC2*, only moderately reduced GSDMD-NT-induced cell death in the LDH assay (fig. S9, C and D) but had no detectable effect on PI

uptake (fig. S9I). We next overexpressed *ZDHHC5* or *ZDHHC9* in HEK293T cells and measured GSDMD palmitoylation with the ABE assay. Compared with control samples, GSDMD palmitoylation significantly increased in cells co-expressing ZDHHC5 (fig. S9J) or ZDHHC9 (fig. S9K).

To validate the physiological significance of ZDHHC5 and ZDHHC9-mediated GSDMD palmitoylation, we used PMA-differentiated macrophage-like THP-1 cells. THP-1 cells expressed both ZDHHC5 and ZDHHC9, and their expression was significantly upregulated at both the mRNA (Fig. 5A and fig. S10A) and protein level (Fig. 5B) following LPS stimulation. ZDHHC5 and ZDHHC9 interacted with GSDMD. Furthermore, this association increased upon LPS stimulation (fig. S10, B to E), likely due to the overall increase in the total amount of ZDHHC5 and ZDHHC9 protein rather than an enhanced binding affinity, since the binding remained unaltered after normalization with the protein input (fig. S10, B to E). Upon stimulation with LPS/Nig, both full-length and cleaved GSDMD-NT were palmitoylated, and siRNA knockdown of *ZDHHC5* or/and *ZDHHC9* significantly suppressed this palmitoylation (Fig. 5, C to E). As a result, cells transfected with *ZDHHC5* or *ZDHHC9* siRNA released less LDH (Fig. 5F) and retained less SYTOX Green nucleic acid stain (Fig. 5G) upon LPS/Nig stimulation. Silencing both *ZDHHC5* and *ZDHHC9* led to almost complete block of GSDMD-NT palmitoylation (Fig. 5E) and more significant reductions in LPS/Nig-induced pyroptotic death compared with silencing each ZDHHC individually (Fig. 5, F and G).

Zdhhc5 and *Zdhhc9* were also expressed in mouse monocytes and macrophages (fig. S10F). We knocked down *Zdhhc5* and *Zdhhc9* with specific siRNAs in mouse primary BMDMs (Fig. 5, H to J). *Zdhhc5* siRNA, but not *Zdhhc9* siRNA, significantly suppressed pyroptosis in mBMDMs as measured by SYTOX Green nuclear staining and LDH release (Fig. 5, H to J). ZDHHC9 protein expression was barely detectable in mBMDMs, potentially explaining why ZDHHC9 knockdown showed no effect (Fig. 5J). In addition, iBMDM expressing GSDMD-NT revealed that ZDHHC5 interacted with GSDMD-NT in mouse macrophages (fig. S1F). Thus, ZDHHC5 and ZDHHC9 are the primary palmitoyl acyl transferases responsible for GSDMD palmitoylation in macrophages, whereas FASN plays a role in catalyzing palmitate biosynthesis, providing the essential substrate for protein palmitoylation. Although siRNA knockdown of *ZDHHC5* and *ZDHHC9* resulted in a significant reduction in palmitoylation of GSDMD, the most substantial inhibition was observed in cells with a triple knockdown of *FASN, ZDHHC5*, and *ZDHHC9* (fig. S2).

GSDMD palmitoylation in macrophages is tightly regulated

GSDMD palmitoylation in macrophages was not constitutive and relied on specific stimuli (Fig. 1, I and J). It could be triggered by LPS alone in the absence of Nig-induced inflammasome activation (Fig. 6A), consistent with a previous study showing that LPS upregulates palmitoyl enzyme transferases in macrophages (52). Significant GSDMD palmitoylation was observed 60 min after LPS stimulation (Fig. 6B). We tested various stimulants, including other TLR agonists, microbial products, and cytokines, in THP-1 cells. LPS and heat-killed *Escherichia coli* induced the most significant increase in GSDMD palmitoylation, whereas the TLR7/8 agonist imidazoquinoline, whole glucan

particles, and IL-6 produced minimal effects (Fig. 6C). A gram-positive bacterium, *Streptococcus pneumoniae*, also induced significant GSDMD palmitoylation, suggesting that this mechanism may extend beyond LPS-induced priming (Fig. 6C).

ROS appeared crucial for LPS-induced GSDMD palmitoylation (fig. S11A and Fig. 6D). An increase in ROS levels resulted in a significant augmentation of GSDMD palmitoylation, although ROS was insufficient to trigger this event in the absence of LPS (Fig. 6D). NF-κB activation was also involved in this process since a specific NF-κB inhibitor (fig. S11B) significantly suppressed LPS-induced GSDMD palmitoylation (Fig. 6D) without producing any detectable cytotoxicity (fig. S11C). To eliminate the possibility that this effect was caused by off-target effects of the inhibitor, a mouse BMDM cell line with a targeted knockout of the NF-κB p50 gene was utilized. We observed comparable outcomes in the NF-κB p50 knockout macrophages to those seen in the macrophages treated with the NF-κB inhibitor (Fig. 6E). Moreover, NF-κB signaling and GSDMD palmitoylation occurred almost simultaneously, highlighting the dynamic relationship between these processes (Fig. 6, B and F). As previously reported, the ROS scavenger N-acetyl-L-cysteine (NAC) significantly suppressed LPS-induced NF-κB signaling, suggesting that its effect on GSDMD palmitoylation might be at least partially mediated by NF-κB (fig. S11B).

We also explored the role of ROS in GSDMD palmitoylation in iBMDMs (fig. S1, A to E). Cellular ROS levels were elevated using rotenone. The increase in ROS level resulted in a significant augmentation of GSDMD palmitoylation and pyroptotic cell death, which could be effectively suppressed by either 2BP or CPP-W (fig. S1, A to E). Thus, ROS play a critical role in GSDMD-NT palmitoylation.

LPS-induced GSDMD-FL palmitoylation was detected even before inflammasome activation (Fig. 6A) and independent of NLRP3 (fig. S11D). In THP-1 cells, significant GSDMD palmitoylation could be induced with a relatively low dose of LPS (100 ng/ml), which coincided with substantial upregulation of *ZDHHC5* and *ZDHHC9* (Fig. 6B). When cells were treated with a high dose of LPS (1 μg/ml), *ZDHHC5* and *ZDHHC9* were only slightly upregulated (fig. S11E) and GSDMD was palmitoylated only at low levels (fig. S11F). In this setting, activation of the inflammasome could further augment GSDMD palmitoylation (fig. S11G). By contrast, GSDMD palmitoylation was not significantly elevated after inflammasome activation in macrophages stimulated with low dose of LPS, where GSDMD palmitoylation was already high even before any stimulation (fig. S11H). These results align with previous studies that show different concentrations of LPS elicit distinct signaling responses in macrophages (53, 54).

GSDMD palmitoylation plays a critical role in pyroptosis initiated by diverse inflammasome stimuli

GSDMD palmitoylation was also upregulated during pyroptosis triggered by AIM2, NLRC4/NAIP, and noncanonical (caspase-11) inflammasome activation (Fig. 6G). Blocking GSDMD palmitoylation significantly suppressed these types of GSDMD-dependent pyroptosis (Fig. 6, I to K). Thus, GSDMD palmitoylation emerges as a universal mechanism that effectively regulates macrophage pyroptosis, serving a pivotal function in pyroptosis induced by diverse inflammasome types.

Inhibition of palmitoylation mitigates sepsis through a GSDMD-dependent mechanism

Gsdmd-deficient mice are protected from sepsis (3, 18, 22, 55–57). We next examined the potential in vivo role of GSDMD palmitoylation in LPS-induced sepsis. GSDMD was robustly palmitoylated upon LPS stimulation, whereas 2BP treatment significantly reduced palmitoylation (fig. S12A). Tumor necrosis factor α (TNF-α), IL-1β, IL-6, and IL-17 levels were all substantially reduced in 2BP-treated mice (fig. S12B), as was LDH release (fig. S12C). All these phenomena were absent in *Gsdmd*-deficient mice, suggesting a specific role for GSDMD in mediating 2BP's effects. We next investigated whether 2BP treatment increased the survival rate of mice subjected to a model of severe sepsis. Following challenge with 25 mg per kilogram of body weight LPS, all WT mice pretreated with phosphate buffered saline (PBS) died within 2 days. By contrast, *Gsdmd*-deficient mice as well as WT mice pretreated with 2BP showed significantly better survival (>70%) than untreated WT mice (fig. S12D). When challenged with 54 mg per kilogram of body weight LPS, even *Gsdmd*-deficient mice had a significant death rate, with about 40% of mice dying within three days. Pretreatment with 2BP failed to improve the survival of *Gsdmd*-deficient mice (fig. S12E). Thus, 2BP-induced protective effects are largely mediated by GSDMD palmitoylation.

We also explored the effect of 2BP on sepsis induced by cecal ligation and puncture (CLP). After CLP, there was a significant increase in cytokine concentrations in WT peritoneal exudate, which was reduced by 2BP treatment (fig. S12F). By contrast, CLP-induced cytokine production was unaffected by 2BP treatment in *Gsdmd*-deficient mice (fig. S12F). Circulating alanine transaminase (ALT), aspartate aminotransferase (AST), blood urea nitrogen (BUN), and creatinine levels were all lower in 2BP-treated mice, which was suggestive of reduced multiorgan dysfunction (fig. S12G). Similarly, peritoneal fluid LDH was reduced in 2BP-treated mice (fig. S12H). Furthermore, semi-quantitative histopathological examination of CLP-challenged mouse lung, kidney, and liver tissue revealed less tissue damage than mock-treated controls (fig. S12, I and J). Consistent with the reduced organ damage, 2BP-treated mice showed significantly improved survival after CLP challenge, >55% survival compared with 0% in the mock-treated mice (fig. S12K). Similar to observations in the LPS sepsis model, all 2BP-induced protective effects were abolished in *Gsdmd*-deficient mice. Thus, because it is a key mechanism regulating GSDMD and pyroptosis, GSDMD palmitoylation is a potential target for the treatment of infectious and inflammatory diseases.

Specific inhibition of GSDMD palmitoylation with CPP-W alleviates sepsis

As a general inhibitor of palmitoylation, 2BP targets multiple proteins. To specifically block GSDMD palmitoylation, we treated mice with the GSDMD palmitoylation–specific competitive peptide CPP-W (Fig. 7) and investigated whether it could alleviate the severity of LPS-induced sepsis. Indeed, due to a reduction in GSDMD-mediated macrophage pyroptosis, serum collected from CPP-W-treated septic mice contained lower levels of pro-inflammatory cytokines IL-1β, IL-6, and TNF-α, confirming attenuated systemic inflammation in these mice compared with PBS or CPP-M controls (Fig. 7A). CPP-W treatment also mitigated the extent of multi-organ dysfunction in septic mice, as evidenced by lower serum ALT, AST, BUN, and creatinine levels (Fig. 7B). Treatment with CPP-W

significantly improved the survival of LPS-challenged mice. At a dose of 25 mg per kilogram of body weight LPS, all control and CPP-M-treated mice died within 48 hours, whereas >70% CPP-W treated mice survived (Fig. 7C). When *Gsdmd* was disrupted, the protective effects of CPP-W treatment were eliminated (Fig. 7D), underscoring GSDMD's role as the mediator of CPP-W's effects. Moreover, these protective benefits were also nullified in mice treated with 2BP (Fig. 7D), providing further confirmation that GSDMD palmitoylation serves as the underlying mechanism for these protective effects. Thus, the specific inhibition of GSDMD palmitoylation may be an effective strategy for the treatment of sepsis.

DISCUSSION

Here we identified palmitoylation of GSDMD on Cys191/192 as a key regulatory mechanism controlling GSDMD activation (Fig. 7E), providing a target for the modulation of immune activity in infectious and inflammatory diseases. A recent study reported a conserved pore-forming domain in bacterial gasdermins (bGSDM) that is stabilized in the inactive state through a buried palmitoyl modification (50). In that study, the S-palmitoylation of bGSDM was unrelated to its membrane localization and pore-forming activity. In another study, palmitoylation of GSDME on its C-terminal (GSDME-CT) was identified during chemotherapy-induced cancer cell pyroptosis. This palmitoylation event hinders the interaction between GSDME-NT and GSDME-CT, facilitating their dissociation and promoting GSDME-NT pore-forming activity (35). This phenomenon differs from the mechanism we now report in the present study. We have determined that GSDMD palmitoylation itself is unable to overcome the autoinhibition by GSDMD-CT in the absence of caspase cleavage and palmitoylation of GSDMD-NT does not impact its interaction with GSDMD-CT.

GSDMD palmitoylation is tightly regulated. Although GSDMD could be spontaneously palmitoylated in HEK293T, HAP, and iBMDM cells, its palmitoylation in human macrophage-like THP-1 cells and mBMDMs only occurred in certain stimulatory contexts. The variation in GSDMD palmitoylation levels among different cell types may be attributed to differences in the expression of genes associated with GSDMD palmitoylation, including *ZDHHC5* and *ZDHHC9* as well as *FASN*, which displayed significant variability across various cell types (fig. S13, A and B). Moreover, ROS may also play a role. For instance, in differentiated THP-1 cells, LPS significantly elevated ROS levels, which could be responsible for inducing GSDMD palmitoylation. By contrast, compared to THP-1 cells, iBMDMs exhibited considerably higher basal ROS levels, which may contribute to the observed increased GSDMD palmitoylation in these cells even in the absence of any stimulation (fig. S11A).

How does palmitoylation dictate GSDMD-NT function and regulate pyroptosis in macrophages? Palmitoylation regulates the hydrophobicity of soluble and membrane proteins (58–61). Consequently, palmitoylation of GSDMD may directly modulate the hydrophobic matching of protein molecules, enhancing their association with membranes and facilitating pore formation by GSDMD. Although GSDMD-NT can directly bind to lipids such as phosphatidylinositol phosphates in the cell membrane inner leaflet, we

argue that S-palmitoylation is also required to stably anchor cleaved GSDMD-NT to the membrane, facilitating plasma membrane rupture and pyroptotic cell death. Notably, Cys191/192 in GSDMD is located in a disordered loop region and exposed to the solvent, making it easily accessible for palmitoylation (7, 15). Additionally, in the GSDMD-NT pore, Cys191/192 is right at the tips of the β-barrel that forms the pore, further supporting its involvement in anchoring the cleaved protein to the membrane (15) (fig. S13, C and D). Palmitoylation of GSDMD-NT indeed enhanced its binding affinity to phosphatidylinositol phosphates and cardiolipin. Cys191 of human GSDMD is positioned adjacent to Leu192, which serves as the contact point for the C-terminal domain of GSDMD responsible for autoinhibition. Mutation of Leu192 hinders the binding of GSDMD-NT to membrane lipids (13). One open question remains whether the impact of GSDMD palmitoylation on Cys191 is connected to this phenomenon. GSDMD-NT accumulates at the mitochondria after AIM2 inflammasome activation (62). Activated gasdermins cause rapid, cardiolipin-dependent mitochondrial destruction, which is crucial for cell death and necessary for IL-1 secretion (63). In line with these observations, we investigated the impact of GSDMD palmitoylation on its mitochondrial localization in mBMDMs and found that palmitoylation was also required for the LPS/Nig-induced mitochondrial localization of GSDMD-NT (fig. S13E), likely mediated through its binding to cardiolipin (Fig. 4, A and B). Inhibition of GSDMD-NT palmitoylation with 2BP resulted in a significant decrease in the translocation of GSDMD-NT to the mitochondria.

GSDMD-FL palmitoylation appears to be a key molecular event in macrophage priming. Both GSDMD-FL and GSDMD-NT could undergo palmitoylation. The cleavage of GSDMD induced by the inflammasome was not a prerequisite for its palmitoylation, and NLRP3 was not involved in GSDMD palmitoylation. LPS alone, even in the absence of nigericin and inflammasome activation, induced GSDMD palmitoylation. Notably, similar observations have been reported for MyD88. LPS stimulation alone leads to MyD88 palmitoylation, independent of inflammasome activation (31). Based on these findings, we propose a model wherein the palmitoylation of GSDMD in macrophages serves as a key molecular event in macrophage priming (Fig. 7E). Priming with LPS can effectively prepare GSDMD for membrane localization, even before its cleavage by caspase 1/11, thus ensuring efficient GSDMD activation and its subsequent pore-forming activity on the membrane following its cleavage by caspase 1/11. The differential effects of low and high doses of LPS on GSDMD-FL palmitoylation during macrophage priming suggest that GSDMD palmitoylation may also serve as a mechanism involved in regulating innate adaptation to varying strengths of stimulants.

MATERIALS AND METHODS

Study design

This study investigated the role of GSDMD palmitoylation in regulating macrophage pyroptosis. GSDMD palmitoylation was assessed using both acyl biotin exchange (ABE) and click chemistry approaches. Mass spectrometry was employed to confirm the palmitoylation site. Pyroptosis was evaluated using the LDH cytotoxicity assay, cytokine measurements, and immunofluorescence imaging in various cell types, including

HEK293T, macrophage-like THP-1 cells, Dox-inducible HAP1-iGSDMD-NT cells, primary mouse bone marrow-derived macrophages, and mouse immortalized bone marrow-derived macrophages (iBMDMs). WT and *Gsdmd*$^{-/-}$ C57BL/6J mice were used to gauge the significance of GSDMD palmitoylation in LPS and cecal ligation and puncture (CLP)-induced sepsis models. The group sizes and the number of repetitions are provided in the figure legends. The sample size was determined based on best practices to ensure sufficient data for robust assessments. Imaging was carried out and analyzed blindly and automatically using a Confocal Zeiss LSM 710 system. Histological evaluations were overseen by an experienced pathologist who was blinded to genotype and treatment. Each experiment adhered to consistent analytical methods.

Mice strains and maintenance

Male 6–8-week-old C57BL/6J mice were purchased from the Jackson Laboratory (Bar Harbor, ME). *Gsdmd*$^{-/-}$ mice (18) (on C57BL/6J background) were inbred and maintained in a pathogen-free system. For studies related to LPS or CLP-induced sepsis, 8–10-week-old male mice were used. For in vitro studies, 8–10-week-old mice of both sexes were used. All mice were housed and cared for in approved veterinary facilities located within Boston Children's Hospital, which provides sterile isolator cages with fresh food, water, and bedding weekly. All animal experiments were conducted in accordance with the Animal Welfare Guidelines of the Boston Children's Hospital. The Boston Children's Hospital Animal Care and Use Committee approved and monitored all procedures.

Reagents and antibodies

Protease inhibitor cocktail and PMSF were purchased from Thermo Fisher Scientific (Waltham, MA; 78440 and 36978). N-ethylmaleimide (04259), cerulenin (C2389), 2-bromopalmitate (21604), hydroxylamine solution (467804), and palmostatin B (178501) were from Sigma-Aldrich (St. Louis, MO). Biotin HPDP (16459), biotin azide (13040), and palmitic acid alkyne (13266) were purchased from Cayman Chemical Company (Bar Harbor, ME). The click chemistry protein reaction buffer kit (C10276) was from Thermo Fisher Scientific. HKEB (Heat Killed *E.coli* 0111:B4), ultrapure LPS, and nigericin were purchased from InvivoGen (San Diego, CAA). Alexa Fluor 488–conjugated goat anti-mouse IgG (H+L) secondary antibody (A32723), Alexa Fluor 594–conjugated goat anti-rabbit IgG secondary antibody (A-11012), and Alexa Fluor 647–conjugated wheat germ agglutinin (W32466) were from Thermo Fisher Scientific. SuperSignal West Femto Maximum Sensitivity Substrate (34096) was from Thermo Fisher Scientific. A list of primary antibodies used is provided in table S2.

Cell-permeable peptide synthesis

Cell-permeable GSDMD-competing and control peptides (CPPs) corresponding to mouse GSDMD (aa 187–197) were chemically synthesized and conjugated with CPP-R9 (D-form) at LifeTein (Somerset, NJ). The purity and sequence of the peptides were verified by mass spectrometry. Prior to experiments, CPPs were dissolved in RNAse-free water to produce a 20-mM stock which was then directly added to the culture media to reach the final designated concentrations.

Cell culture

HEK293T and THP-1 cell lines were purchased from the ATCC. HAP1 was procured from Horizon Discovery (Cambridge, UK). NFKB p50 KO (C57/129) macrophage cell line (ENH180-FP) was purchased from Kerafast (Shirley, MA). THP-1-Lucia™ NF-κB (thpl-nfkb) and THP-1-KO-NLRP3 (thp-konlrp3z) cell lines were purchased from Invivogen (San Diego, CA). HEK293T, THP-1, and HAP1 cells were cultured in DMEM, RPMI-1640, and IMDM media (Thermo Fisher Scientific), respectively. For routine maintenance, the medium was supplemented with 10% fetal bovine serum (FBS), penicillin (100 U/ml), and streptomycin (100 μg/ml) (Thermo Fisher Scientific). The cells were then cultured at 37°C under 5% CO_2.

Detection of GSDMD palmitoylation by acyl biotin exchange (ABE)

To detect palmitoylation, cells were lysed with lysis buffer (50 mM Tris pH 7.2, 150 mM NaCl, 1% NP-40, and 1 mM EDTA) containing 20 mM N-ethylmaleimide (NEM) and 1X Halt™ Protease Inhibitor Cocktail (Thermo Fisher Scientific). Samples were incubated for 2 hours with agitation at 4°C and then centrifuged at 16,000*g* for 15 min. The protein concentration was determined prior to ABE. Two hundred microliters of protein was precipitated with methanol (800 μl)–chloroform (200 μl)–water (600 μl). The resulting pellet was dissolved in 100 μl of 1% SDS solution, followed by incubation with 400 μl lysis buffer with or without 0.5 M hydroxylamine (HAM, Sigma Aldrich). After 1 hour incubation at RT, proteins were precipitated again. The pellet was dissolved in 100 μl of 1% SDS, followed by incubation with 400 μl of 4 mM biotin HPDP (Thermo Fisher Scientific) in lysis buffer for 1 hour at RT. After the incubation, proteins were precipitated. The pellet was dissolved in 100 μl of lysis buffer containing 1% SDS and diluted 1:10 with PBS, and 30 μl of streptavidin agarose beads (Thermo Fisher Scientific) were added and incubated overnight at 4°C. Beads were washed four times with lysis buffer and proteins were eluted with 50 μl of 2X SDS-Laemmli buffer containing 5% β-mercaptoethanol (BioRad Laboratories) in a boiling water bath for 5 min. Proteins were separated by 4 to 15% gradient SDS-PAGE (BioRad Laboratories).

Detection of GSDMD palmitoylation by click chemistry

HEK293T cells were treated with alkyne-palmitic acid (20 μM) for 24 hours in 10% charcoal-stripped FBS medium (Thermo Fisher Scientific). Cells were lysed in lysis buffer (50 mM Tris pH 7.2, 150 mM NaCl, 10% glycerol, 1% NP-40, and 1 mM EDTA) and the cell lysates were centrifuged at 16,000*g* for 15 min. The proteins in the supernatant were quantified and precipitated as described in the ABE method. The pellet was dissolved in 60 μl of 1% SDS and subjected to a click chemistry reaction using the Click-iT Protein Buffer kit (Thermo Fisher Scientific). The 60 μl protein sample was mixed with 100 μl of clickIT reaction buffer containing 5 mM biotin azide, 10 μl CuSO4, 10 μl click it reaction buffer additive 1, and 20 μl buffer addtive2 solution, and incubated for 30 min at RT. Proteins were then precipitated again with Methanol (800 μl)-Chloroform (200 μl)-water (600 μl), and the pellets were dissolved in 100 μl of 1% SDS and incubated with or without 0.5 M HAM in 400 μl lysis buffer for 1 hour at RT. After the incubation, proteins were precipitated. The pellet was dissolved in 100 μl of lysis buffer containing 1% SDS and diluted 1:10 with

PBS. Thirty microliters of streptavidin agarose beads (Thermo Fisher Scientific) was then added and the mixture was incubated overnight at 4°C. Beads were washed four times with lysis buffer and proteins were eluted with 50 μl of 2X SDS-Laemmli buffer containing 5% β-mercaptoethanol (BioRad Laboratories) in a boiling water bath for 5 min.

Detection of GSDMD oligomerization

To examine the effect of palmitoylation inhibition on GSDMD oligomerization, HEK293T cells were transiently transfected with FLAG-GSDMD-NT (WT) or FLAG-GSDMD-NT-C192A. After 4 hours of transfection, cells were treated with or without 2BP (50 μM) or CPP-W (50 μM). After 24 hours, cells were lysed in non-denaturing lysis buffer (20 mM Tris HCl pH 8, 137 mM NaCl, 1% Triton X-100, and 2 mM EDTA). Protein samples were then separated using non-denaturing PAGE (Mini-PROTEAN TGX Stain gel, Biorad). Immunoblots were performed with anti-FLAG antibody.

LPS-induced sepsis model

Sepsis was induced in 6-week-old C57BL/6 mice and *Gsdmd*$^{-/-}$ mice by intraperitoneal injection of LPS (25 mg per kilogram of body weight). Before LPS injection, mice were treated with 2-bromopalmitate (30 mg per kilogram of body weight). To assess the severity of sepsis, the overall inflammatory response was evaluated by measuring the concentrations of inflammatory cytokines in both plasma and peritoneal fluid using enzyme-linked immunosorbent assay (ELISA) (Thermo Fisher). Blood was collected via retro-orbital bleeding into EDTA-supplemented blood collection tubes (BD Microtainer tubes). The plasma was separated from the blood by centrifuging the samples at 6000*g* for 5 min. The separated plasma was then diluted with a sample diluent provided by the company (Thermo Fisher, MA) at a minimum ratio of 1:5, and cytokines were quantified using the standard ELISA procedure according to the manufacturer's protocol (Thermo Fisher). The peritoneal fluid was collected by lavaging the peritoneal cavity twice, each time with 3 ml of PBS. Afterward, the fluid was centrifuged at 400*g* for 5 min, and the supernatant was collected for cytokine measurement and LDH release assay (Promega LDH-Glo cytotoxicity assay). To confirm GSDMD palmitoylation in vivo in septic mice, peritoneal cells from LPS-challenged control and 2BP-pretreated mice were collected after 12 hours. GSDMD palmitoylation was assessed using the ABE assay. To examine the effect of CPP peptides on sepsis, C57BL/6J mice were pretreated with CPP-W (50 mg per kilogram of body weight, i.p.) or CPP-M (50 mg per kilogram of body weight, i.p.) for 6 hours, followed by intraperitoneal challenge with indicated dose of LPS for 12 hours.

Cecal ligation and puncture

Cecal ligation and puncture (CLP) was performed as previously described with minor modifications (64, 65). Briefly, knockout and WT mice of matched age and sex were anesthetized with a mixture of xylazine (10 mg per kilogram of body weight) and ketamine (100–120 mg per kilogram of body weight). The surgical area was prepared by applying hair removal cream to remove hair from the abdominal region, followed by sterilization with iodine and alcohol-soaked pads. A ventral midline incision was made on the skin and then on the peritoneum to expose the cecum. The cecum was ligated approximately 1–1.5 inches from its blunt end and two perforations were made on the cecum using an

18G needle to induce a severe sepsis. After expressing a small amount of cecal contents into the peritoneal cavity, the cecum was repositioned to its original place. The peritoneum was sutured, and tissue clips were used to close the skin. A subcutaneous injection of one milliliter of normal saline into the loose skin around the neck area was administered to each mouse to compensate for fluid loss during surgery.

Cell fractionation

Cell cytoplasmic and membrane fractions were prepared using a Cell Fractionation Kit (Cell Signaling Technology). Briefly, HEK293T cells (2.2×10^6) were seeded in a 100-mm cell culture plate. After 24 hours of transfection with mGSDMD-NT or mGSDMD-C192A cDNA, cells were washed with PBS, trypsinized with 0.25% trypsin–EDTA (Thermo Fisher Scientific) and then collected by centrifugation at 400*g* for 5 min. Cells were then lysed with 500 μl of cytoplasmic isolation buffer, vortexed, and incubated on ice for 5 min followed by centrifugation at 500*g* for 5 min. The supernatant was collected as a cytoplasmic fraction. The remaining pellet was resuspended in 500 μl of membrane isolation buffer and incubated on ice for 5 min. After centrifugation at 8000*g* for 5 min, the supernatant was collected and stored at −80°C as a membrane fraction.

Cloning and mutagenesis

cDNA clones from mouse and human *GSDMD* were cloned into pCDNA vectors. FLAG-gasdermin D-C-terminus was purchased from Genscript Biotech Corp (Piscataway, NJ). FLAG-GSDMD-FL-C192A was purchased from Genscript. HA-tagged DHHC 1–23 plasmids were obtained from M. Fukata, Japan. FLAG-N-*Gsdmd* wild-type and FLAG-*Gsdmd*-NT mouse mutants C39A, C57A, C77A, C122A, C192A, and C265A were generated as previously described (10).

Coimmunoprecipitation to isolate GSDMD-binding proteins

Cells were washed with PBS and lysed with lysis buffer (50 mM Tris pH 7.4, 150 mM NaCl, 1 mM EDTA, and 1% NP-40) containing protease inhibitor and incubated for 30 min in ice. Briefly, cell lysates were centrifuged at 16,000*g* for 10 min. Protein in the supernatant was quantified with a Bradford assay. Cell lysates with or without anti-FLAG M2 agarose beads were incubated overnight at 4°C with gentle rocking. After 24 hours, samples were centrifuged at 6000*g* and washed at least three times with lysis buffer (50 mM Tris pH 7.4, 150 mM NaCl, 1 mM EDTA, and 1% NP-40) Proteins were eluted with 0.2 M glycine (pH 2.0) and samples were processed for mass spectrometry and immunoblotting.

Identification of GSDMD-binding proteins by mass spectrometry

Mass spectrometry (MS)—Immunoprecipitated protein samples were concentrated using a speed vacuum concentrator and samples were further dissolved in 100 μl of triethylammonium bicarbonate (TEAB) heated to 95°C for 5 min and cooled to room temperature (RT). In-solution proteins were digested with trypsin–LysC (1:50 ratio) (6 μg, Thermo Fisher Scientific) and incubated at 37°C for 3 hours. Digested proteins were desalted using a c18 spin column (Thermo Fisher Scientific The analysis was conducted using an Orbitrap Elite Hybrid Ion Trap-Orbitrap Mass Spectrometer (Thermo Fisher, San

Jose, CA) coupled with a nano pump from Waters Acquity (WATERS Corp., Milford, MA) for liquid chromatography. The peptide separation process utilized a microcapillary column with an internal diameter of 100 μm. This column was initially packed with C18 Reprosil resin (5 μm particle size, 100 Å pore size, Dr. Maisch GmbH, Germany) for about 5 cm, which then led into an analytical column provided by WATERS. A gradient of 5% to 27% acetonitrile (ACN) in 0.1% formic acid was employed over a 90-min period at a flow rate of 200 nl/min to achieve peptide separation. Electrospray ionization was facilitated using a 1.8 kV voltage, applied through a custom electrode junction at the column's end. The Orbitrap Velos operated in a data-dependent acquisition mode, conducting an initial mass spectrometry scan in the Orbitrap across a mass-to-charge (m/z) range of 395 to 1,800 at a 60,000 resolution. This was followed by CID-MS^2 fragmentation of the top thirty ions (TOP30) in the Ion trap, utilizing a 2 m/z precursor isolation window, an Automatic Gain Control (AGC) of 10,000, and a maximum ion accumulation time of 200 ms. Ions with a single charge were excluded from CID fragmentation.

Mass spectrometry data analysis—For the analysis of mass spectrometry data, the raw files were processed using Proteome Discoverer 2.4 (Thermo Scientific) software. The Sequest HT algorithm facilitated the assignment of MS/MS spectra by comparing against a protein sequence database that included entries from the Uniport_Human2016_SPonly database alongside known contaminants such as human keratins and typical laboratory contaminants. The search parameters set for Sequest HT included a precursor ion tolerance of 20 ppm, adherence to Trypsin protease specificity at peptide N-/C- termini with up to two missed cleavages allowed. To ensure data integrity, a false discovery rate (FDR) of 1% was maintained for both protein and peptide identifications through a target-decoy search strategy. Data filtering employed the Percolator (64-bit version) tool. Specificity in the analysis was further enhanced by setting static modifications for peptide N termini and lysine residues (+229.162932 Da) and variable modifications for methionine oxidation (+15.99492 Da), ensuring a comprehensive and accurate representation of the sample's proteomic profile.

Identification of GSDMD palmitoylation site by mass spectrometry

We used immunoprecipitation and a well-established acyl–biotinyl exchange (ABE)-based proteomic protocol to purify and identify palmitoylated GSDMD from complex protein extracts. The method relies on an ABE chemistry to irreversibly replace the thioester-linked palmitoyl modifications with stable biotin tags. The blockage of all free thiol groups was achieved by treatment with N-ethylmaleimide (NEM). The palmitoyl group was then removed from cysteines via hydroxylamine-induced hydrolysis, followed by labeling of the newly freed thiol groups with HPDP-Biotin (Thermo Scientific). The biotinylated proteins were then affinity-purified using streptavidin–agarose beads, trypsin digested, and subjected to LC–MS/MS analysis (66).

Acyl–biotinyl exchange chemistry—HEK293T cells were transiently transfected with a FLAG-GSDMD-NT construct. After 24 hours, the cells were washed and lysed with lysis buffer containing NEM (150 mM NaCl, 50 mM Tris, 5 mM EDTA, pH 7.4, 10 mM NEM, 2X protease inhibitors, 2 mM PMSF, and 2X phosphatase inhibitor) and incubated

with rotation at 4°C for 2 hours. Following incubation, cell lysates were centrifuged at 16,000*g* for 10 min. The supernatant was incubated with anti-FLAG M2 agarose beads (Sigma Aldrich) overnight at 4°C. After 24 hours, the beads were washed four times with 1X lysis buffer. To elute the proteins, 0.2 M glycine (pH 2.0) was added and incubated for 10 min at room temperature (RT). The supernatant was collected by centrifugation and neutralized with 1 M Tris pH 7.4. Protein from the solution was precipitated using methanol (4 volumes)–chloroform (1.5 volumes)–water (3 volumes) followed by centrifugation at 14,000*g* for 10 min. The interphase was collected and 3 volumes of methanol were added followed by pelleting through centrifugation at 16,000*g* for 10 min. After the third methanol–chloroform (MC) precipitation, the pellet was air-dried and dissolved in 2% sodium dodecyl sulfate (SDS) for 10 min at RT. The samples were then diluted fivefold with lysis buffer containing hydroxylamine (0.7 M) and incubated for 1 hour with rotation at RT. After incubation, the samples were subjected to three rounds of MC precipitation, and the resulting pellets were dissolved in 2% SDS at room temperature for 10 min. The samples were then diluted with lysis buffer containing 1 mM EZ-Link™ HPDP-Biotin (Thermo Scientific) and incubated for 1 hour at RT to label the proteins with biotin. To remove unreactive HPDP-biotin, MC precipitation was performed and the pellets were dissolved in lysis buffer containing 2% SDS. The final SDS concentration was adjusted to less than 0.5% with lysis buffer. Subsequently, 50 μl of streptavidin–agarose beads were added and incubated overnight at 4°C. The beads were washed four times with lysis buffer. To elute the bound proteins from the beads, lysis buffer containing 2% SDS with 1% β-mercaptoethanol was added, and the mixture was incubated for 15 min at RT. The supernatant was collected by centrifugation and the samples were subjected to chloroform/methanol precipitation to isolate proteins. Following precipitation, the proteins were resuspended in 0.2 M glycine (pH 2.0) and subsequently sent to the core facility for MS analysis.

Sample preparation and mass spectrometry—The samples for proteomic mass spectrometry analysis were prepared using established protocols at Harvard Center for Mass Spectrometry. Protein samples were first concentrated using a speed vacuum concentrator, dissolved in 100 μl of TEAB, and then alkylated by iodoacetamide (IAA) at RT for 30 min in the dark. In-solution proteins were digested with trypsin (1:50 ratio) and incubated at 37°C overnight. Digested proteins were desalted using a C18 spin column. The samples were subjected to MS analysis by following the procedure used for identifying GSDMD-binding proteins.

Mass spectrometry data analysis—The raw data were analyzed using Proteome Discoverer 2.5 (Thermo Fisher Scientific) and Byonic v2.0 (Protein Metrics) software, with the Byonic search algorithm integrated as a node in Proteome Discoverer 2.4. Assignment of MS/MS spectra was achieved by employing both the SEQUEST HT and Byonic algorithms, which involved searching the data against a custom protein sequence database and known contaminants, including human keratins and typical laboratory contaminants. The SEQUEST HT searches adhered to a precursor ion tolerance of 10 ppm and enforced trypsin protease specificity for peptide N/C termini, permitting up to two missed cleavages. Variable modifications included oxidation of methionine (+15.995 Da), carbamidomethyl on cysteine (+57.021 Da), N-ethylmaleimide on cysteine (+125.048 Da), and phosphorylation

on serine, threonine, and tyrosine (+79.966 Da). To ensure accuracy, an MS2 spectra assignment false discovery rate (FDR) of 1% was maintained for both protein and peptide levels using a target-decoy database search strategy. The Percolator (64-bit) was utilized for result filtering to maintain the stringent quality of the analysis.

siRNA knockdown

THP-1 and primary bone marrow-derived macrophages (1×10^6 cells/ml) were electroporated using Lonza Bioscience Nucleofector kit (Morrisville, NC; VCA-1003 and VPA-1009) with scramble control RNA and gene-targeting siRNAs (table S3) for 48 hours. For HEK293T cells, siRNA was transfected using Lipofectamine 3000 in HEK293T cells.

Immunoblotting

Cell lysates were lysed in lysis buffer containing 25 mM tris pH 7.4, 150 mM NaCl, 1% NP-40, 10% glycerol, and 1 mM EDTA. Samples were centrifuged at 16,000*g* for 10 min. Lysates were fractionated in 4 to 15% gradient SDS-PAGE (BioRad Laboratories, Hercules, CA). Proteins were then transferred to E-PVDF membranes (Millipore, Burlington, MA) and membranes were probed with primary antibodies (1:100) in 2% BSA in blocking buffer overnight at 4°C. After incubation, blots were washed three times with 1X TBST and probed with secondary HRP-conjugated antibody (1:10,000) for 1 hour at RT. Membranes were washed with TBST and mixed with 1:1 SuperSignal West Femto Max substrate, and chemiluminescence signal was captured using a BioRad Chemidoc XP machine. Band intensities were quantified using ImageJ software. For each blot, the band displaying the strongest intensity was selected for normalization to minimize inter-experimental variation, including signal intensity variations resulting from differing exposure times.

LDH release assay

LDH, a soluble, stable cytosolic enzyme, is rapidly released upon the disruption of the plasma membrane and is commonly used as a marker for cell death. LDH release was measured using a bioluminescent-based LDH-Glo cytotoxicity assay (Promega). Briefly, cell culture supernatants were centrifuged at 16,000*g* for 5 min. Samples were diluted at least 1:100 in LDH storage buffer (200 mM Tris-HCl, pH 7.3, 10% glycerol, 1% BSA). One hundred microliters of the LDH substrate mixture was added to the samples and incubated in the dark at RT for 30 min. Luminescence was then captured using a BioTek Synergy HTX Multimode Reader. The percentage LDH release was then calculated.

Immunofluorescence imaging

To visualize the localization of GSDMD-NT, HEK293T cells were plated on coverslips and transiently transfected with wild-type FLAG *Gsdmd*-NT and mutant FLAG *Gsdmd*-N-C192A. Six hours after transfection, cells were treated with or without 2-bromopalmitate. Twenty-four hours later, cells were washed with PBS and fixed with 3% paraformaldehyde and stained with wheat germ agglutinin, followed by washing and permeabilization for 15 min with 0.5% Triton X-100 (Thermofischer) in PBS. Blocking buffer (2% BSA in PBS) was added to the cells prior to incubation for 30 min. Goat anti-mouse FLAG primary antibody was diluted 1:2000 in blocking buffer and incubated at 4°C overnight. After

three washes in wash buffer (PBS containing 0.1% Tween-20), Alexa Fluor 488-conjugated secondary antibody (1:1000) was added and incubated for another hour at RT. Cells were washed and visualized using a with a Zeiss LSM 980 Confocal Microscope with Airyscan2 and Multiplex Mode (Carl Zeiss Microscopy). Fluorescence filters AF488 (493/520), AF594 (590/619), AF647 (653/669), and DAPI (358/463) were used. The microscope is equipped with blue (488), red (561), violet (405), and far-red (633) solid-state lasers. Images were captured using a Plan-Apochromat 63x/1.4 Oil M27 or a Plan-NEOFLUAR 10x/0.3 objective lens with a Zeiss T-PMT digital detector. Zeiss Zen Black software was used for image acquisition. Images were processed using ImageJ (NIH) software. GSDMD-NT membrane localization was quantified by measuring Pearson's coefficient of GSDMD-NT and wheat germ agglutinin (WGA), a marker for plasma membrane. Colocalization efficiency was quantified with the ImageJ plugin coloc2 with background subtraction and ROI selection. Results are presented as normalized Pearson's correlation.

Dox-inducible system (HAP1-iGSDMD-NT cells)

cDNA encoding human gasdermin D N terminal region (1–275) was amplified and cloned into the pLVX Tet plasmid. To generate stable expression of GSDMD-NT, the pLVX tetone-hGsdmd-1–275-2A-GFP-IRES-Blast vector was transfected into HAP1 cells with Lipofectamine 2000 and selected with blasticidin for 24 and 48 hours. Single cell clones were obtained and screened for GFP by FACS. To confirm gene expression of GSDMD-NT, cells were treated with doxycycline (10–100 ng/ml) for 1–6 hours. After Dox stimulation, cell death was observed by fluorescence microscopy with propidium iodide (PI) (BD Biosciences) staining. GFP-positive signal and PI-positive cells were captured and quantified using ImageJ. Media supernatants were collected and quantified for LDH release. HAP1 cells expressing inducible GFP (HAP1-iGFP) were used as a control for this study.

Real-time PCR

Total RNA was isolated using the Qiagen RNeasy Mini kit (Qiagen, Hilden, Germany). Using a cDNA synthesis kit (Bio-Rad), RNA was reverse-transcribed into cDNA. cDNA was amplified using a Bio-Rad CFX 96 real-time PCR detection system using primers indicated in table S4. Gene expression was normalized to a *Gapdh* loading control.

Primary mouse bone marrow-derived macrophages and pyroptosis assay

Wild-type and *Gsdmd*$^{-/-}$ bone marrow was isolated as described previously (55). Bone marrow cells were isolated and seeded into six-well plates. They were maintained in DMEM containing 10% FBS, 100 U/ml of penicillin–streptomycin with 30 ng/ml of recombinant M-CSF and incubated for 6 days. The medium was changed every 3 days. On day 6, adherent macrophages were washed once with DMEM, and cells were primed with LPS (1 μg/ml) for 3 hours followed by secondary stimulation with 20 μM nigericin for 1 hour. The supernatant was removed and quantified for LDH release. The remaining cells were stained with STOX green (1:30,000)(Thermo Fischer) and PI (BD Biosciences) Fluorescence signals were captured and images were quantified using ImageJ.

Mouse immortalized bone marrow–derived macrophages

Immortalized bone marrow–derived macrophages (iBMDMs) were generated as previously described (23) and cultured using DMEM with Glutamax, supplemented with 10% fetal bovine serum (FBS) and 1% penicillin–streptomycin. For the doxycycline (Dox)–inducible cell lines, the cells were cultured in the presence of puromycin (10 μg/ml) and G418 (1.5 μg/ml). To induce the expression of GSDMD-NT, doxycycline (0.5 μg/ml) was added to the cells in serum-free media. The cells were then incubated for 4–6 hours, after which cell death assays were performed. To examined whether GSDMD was localized to the mitochondria, iBMDMs constitutively expressing GSDMD-FL (23) were primed with LPS (1 μg/ml) for 3 hours, followed by a 30-min treatment with 2BP. The cells were then stimulated with nigericin (10 μM) for 20 min. Mitochondria staining was performed using MitoTracker™ Red FM (Thermofisher) and GSDMD was detected via immunostaining with an anti-GSDMD antibody.

Lipid-binding assay

HEK293T cells were transiently transfected with GSDMD-FL and GSDMD-NT constructs. After 24 hours, the cells were washed with 1X DPBS and lysed with 1X lysis buffer containing 50 mM Tris (pH 7.4), 150 mM NaCl, 0.5% NP-40, 2 mM EDTA, and 1X proteinase and phosphatase inhibitor on ice for 30 min. Subsequently, the samples were centrifuged at 16,000*g* for 10 min. The supernatant was collected and incubated with lipid (PtdIns(4)P, PtdIns(4,5)P, cardiolipin, or phosphatidylcholine)–conjugated agarose beads (Echelon Biosciences) overnight at 4°C. Following the incubation, the beads were washed four times with lysis buffer. To elute the bound proteins, 50 μl of 2X SDS-PAGE loading buffer was added to the beads, which were then incubated in a 95°C water bath for 5 min. Samples were centrifuged at 16,000*g* for 2 min and then separated by SDS-PAGE and subjected to immunoblot analysis using a goat anti-FLAG-HRP antibody (Sigma-Aldrich).

NF-κB reporter activity assay

THP-1-Lucia™ NF-κB cells (Invivogen) were cultured in RPMI 1640 media supplemented with 2 mM L-glutamine, 25 mM HEPES, 10% heat-inactivated FBS, 100 μg/ml of Normocin™, penicillin (100 U/ml), and streptomycin (100 μg/ml). To induce NF-κB reporter activity, THP-1 cells were stimulated with or without LPS (100 ng/ml) for the specified time points. For the luciferase assay, the required volume of QUANTI-Luc™4 Reagent (Invivogen) was prepared. The luminometer was set up with the following parameters: 50 μl of Luc reagent with a 4 second-integration time. Prior to the measurements, the injector was primed with the reagents, and RFU (Relative Fluorescence Units) measurements were determined using a BioTek Synergy HTX Multimode Reader.

Coimmunoprecipitation to assess FASN-GSDMD interaction

Purified recombinant c-Myc-tagged FASN protein was diluted in 1X lysis buffer, with or without recombinant His-tagged hGSDMD-FL protein, along with actin and GFP (as controls), and incubated with 50 μl of Dynabeads™ His-Tag Isolation and Pulldown beads (Thermo Fisher) overnight. After washing, proteins were directly eluted with elution buffer containing 300 mM imidazole (Sigma Aldrich). Eluted protein samples were subjected

to Immunoblot analyses with anti-GSDMD and other indicated antibodies as previously described. To examine FASN-GSDMD interaction in HEK293T cells, cells transfected with or without hGSDMD-FL-FLAG were coimmunoprecipitated with anti-FLAG antibodies, and immunoblot analyses were performed with anti-FLAG HRP antibodies. To examine FASN-GSDMD interaction in THP-1 cells, PMA-differentiated THP-1 cells were treated with or without LPS (1 μg/ml) for 3 hours. Cells were lysed, and immunoprecipitation was performed with anti-rabbit GSDMD-FL antibody followed by immunoblot analysis.

Histological staining and scoring

Tissue samples from the lung, kidney, and spleen were fixed in 4% paraformaldehyde (PFA), followed by a step-wise dehydration process before being embedded in paraffin. Sections of the tissues, 4 μm-thick, were then prepared and subjected to hematoxylin and eosin (H&E) staining for examination under a light microscope. The evaluation of lung tissue damage was performed using criteria that included alveolar capillary congestion, hemorrhage, edema, infiltration by inflammatory cells, structural integrity, and the thickness of the alveolar walls. For kidney tissues, assessments were made based on capillary congestion, hemorrhage, edema, infiltration by inflammatory cells, dilation and degeneration of tubules, and necrosis. Spleen tissue evaluation focused on morphological signs of apoptosis such as cellular shrinkage and nuclear condensation. The extent of these characteristics was quantified using a scoring system ranging from 0 to 10, where 0 indicated the absence (normal condition) and scores from 1–4, 5–6, 7–8, and 9–10 corresponded to mild (10 to 40%), moderate (50 to 60%), severe (70 to 80%), and very severe (90 to 100%) damage, respectively. An experienced pathologist, blinded to genotypes and treatments, carried out the histological scoring.

Illustration of Cys191 in the auto-inhibited full-length GSDMD and the GSDMD-NT pore structures

The available crystal structure of GSDMD (PDB: 6n9o) does not contain the C191 region (7). A homology model of full-length human GSDMD was generated by SWISS-Model (66) based on 6n9o. Electron microscopy imaging of GSDMD-NT pore, data processing, model building, and structure analysis were essentially conducted as previously described (15).

Quantification and statistical analysis

All experiments were performed independently at least three times and the data were pooled and analyzed together. No samples or animals subjected to successful procedures and/or treatments were excluded from the analyses. A two-tailed, unpaired Student's *t* test was employed to test for statistical significance between two groups. One-way (for experiments with one variable) or two-way (for experiments with two variables) analysis of variance (ANOVA) followed by Bonferroni's multiple comparison test was utilized when comparing more than two groups. Values shown in each figure represent mean ± SEM. A *P*-value of <0.05 was considered statistically significant. For mouse survival analysis, Kaplan–Meier survival curves were generated using survival data and groups were compared by log-rank (Mantel–Cox) test. All statistical analyses and graphics were generated using GraphPad Prism (GraphPad, San Diego, CA).

Supplementary Material

Refer to Web version on PubMed Central for supplementary material.

Acknowledgements

The authors thank T.S. Xiao, M.D. Resh, L. Li, J.A. Cancelas, Y. Zheng, B.C. Dickinson, and L. Chai for helpful discussions and suggestions. We also thank R. Robinson, S. Kolakowski, B. Budnik, and M. Chen at the HMS Proteomics Core Facility for MS data collection and analysis, and E. Liu at the Harvard Catalyst Biostatistical Consulting Program for assistance with statistical analyses. We thank the IDDRC Cellular Imaging Core, funded by NIH grants P50 HD105351 and NIHS10OD030322 for the use of the Zeiss LSM 980 microscope.

Funding:

H.R.L was supported by National Institutes of Health grants 1R01AI142642, 1R01AI145274, 1R01AI141386, R01HL092020, and P01HL158688. J.C.K. was supported by NIH grants AI133524, AI116550, and P30DK34854. H.W. was supported by NIH grants AI139914, DP1HD087988, and AI124491. A.H. was supported by NIH training grant T32HL066987. P.D. was supported by a PhD fellowship from the Boehringer Ingelheim Fonds.

Data and materials availability:

Mass spectrometric data have been deposited to ProteomeXchange Consortium with the dataset identifier PXD039133. GSDMD-Flag, GFP-FLAG, and actin-interacting proteins identified using mass spectrometry (Fig. 1A and table S1) are archived in data S1. The high-confidence peptides corresponding to portions of GSDMD-NT identified by LC–MS/MS, as described in Fig. 3D, are archived in data S2. All other data needed to evaluate the conclusions in the paper are present in the paper and/or the Supplementary Materials, including raw data used to generate all figures (data S3 and S4).

REFERENCES AND NOTES

1. Jorgensen I, Miao EA, Pyroptotic cell death defends against intracellular pathogens. Immunol Rev 265, 130–142 (2015). [PubMed: 25879289]
2. Man SM, Karki R, Kanneganti TD, Molecular mechanisms and functions of pyroptosis, inflammatory caspases and inflammasomes in infectious diseases. Immunol Rev 277, 61–75 (2017). [PubMed: 28462526]
3. Shi J, Zhao Y, Wang K, Shi X, Wang Y, Huang H, Zhuang Y, Cai T, Wang F, Shao F, Cleavage of GSDMD by inflammatory caspases determines pyroptotic cell death. Nature 526, 660–665 (2015). [PubMed: 26375003]
4. Kayagaki N, Stowe IB, Lee BL, O'Rourke K, Anderson K, Warming S, Cuellar T, Haley B, Roose-Girma M, Phung QT, Liu PS, Lill JR, Li H, Wu J, Kummerfeld S, Zhang J, Lee WP, Snipas SJ, Salvesen GS, Morris LX, Fitzgerald L, Zhang Y, Bertram EM, Goodnow CC, Dixit VM, Caspase-11 cleaves gasdermin D for non-canonical inflammasome signalling. Nature 526, 666–671 (2015). [PubMed: 26375259]
5. He WT, Wan H, Hu L, Chen P, Wang X, Huang Z, Yang ZH, Zhong CQ, Han J, Gasdermin D is an executor of pyroptosis and required for interleukin-1beta secretion. Cell Res 25, 1285–1298 (2015). [PubMed: 26611636]
6. Broz P, Pelegrin P, Shao F, The gasdermins, a protein family executing cell death and inflammation. Nat Rev Immunol 20, 143–157 (2020). [PubMed: 31690840]
7. Liu Z, Wang C, Yang J, Zhou B, Yang R, Ramachandran R, Abbott DW, Xiao TS, Crystal Structures of the Full-Length Murine and Human Gasdermin D Reveal Mechanisms of Autoinhibition, Lipid Binding, and Oligomerization. Immunity 51, 43–49.e44 (2019). [PubMed: 31097341]

8. Shi P, Tang A, Xian L, Hou S, Zou D, Lv Y, Huang Z, Wang Q, Song A, Lin Z, Gao X, Loss of conserved Gsdma3 self-regulation causes autophagy and cell death. Biochem J 468, 325–336 (2015). [PubMed: 25825937]

9. Man SM, Kanneganti TD, Gasdermin D: the long-awaited executioner of pyroptosis. Cell Res 25, 1183–1184 (2015). [PubMed: 26482951]

10. Liu X, Zhang Z, Ruan J, Pan Y, Magupalli VG, Wu H, Lieberman J, Inflammasome-activated gasdermin D causes pyroptosis by forming membrane pores. Nature 535, 153–158 (2016). [PubMed: 27383986]

11. Sborgi L, Ruhl S, Mulvihill E, Pipercevic J, Heilig R, Stahlberg H, Farady CJ, Muller DJ, Broz P, Hiller S, GSDMD membrane pore formation constitutes the mechanism of pyroptotic cell death. EMBO J, (2016).

12. Aglietti RA, Estevez A, Gupta A, Ramirez MG, Liu PS, Kayagaki N, Ciferri C, Dixit VM, Dueber EC, GsdmD p30 elicited by caspase-11 during pyroptosis forms pores in membranes. Proc Natl Acad Sci U S A 113, 7858–7863 (2016). [PubMed: 27339137]

13. Ding J, Wang K, Liu W, She Y, Sun Q, Shi J, Sun H, Wang DC, Shao F, Pore-forming activity and structural autoinhibition of the gasdermin family. Nature 535, 111–116 (2016). [PubMed: 27281216]

14. Chen X, He WT, Hu L, Li J, Fang Y, Wang X, Xu X, Wang Z, Huang K, Han J, Pyroptosis is driven by non-selective gasdermin-D pore and its morphology is different from MLKL channel-mediated necroptosis. Cell Res 26, 1007–1020 (2016). [PubMed: 27573174]

15. Xia S, Zhang Z, Magupalli VG, Pablo JL, Dong Y, Vora SM, Wang L, Fu TM, Jacobson MP, Greka A, Lieberman J, Ruan J, Wu H, Gasdermin D pore structure reveals preferential release of mature interleukin-1. Nature 593, 607–611 (2021). [PubMed: 33883744]

16. Sollberger G, Choidas A, Burn GL, Habenberger P, Di Lucrezia R, Kordes S, Menninger S, Eickhoff J, Nussbaumer P, Klebl B, Kruger R, Herzig A, Zychlinsky A, Gasdermin D plays a vital role in the generation of neutrophil extracellular traps. Science immunology 3, (2018).

17. Orning P, Weng D, Starheim K, Ratner D, Best Z, Lee B, Brooks A, Xia S, Wu H, Kelliher MA, Berger SB, Gough PJ, Bertin J, Proulx MM, Goguen JD, Kayagaki N, Fitzgerald KA, Lien E, Pathogen blockade of TAK1 triggers caspase-8-dependent cleavage of gasdermin D and cell death. Science 362, 1064–1069 (2018). [PubMed: 30361383]

18. Kambara H, Liu F, Zhang X, Liu P, Bajrami B, Teng Y, Zhao L, Zhou S, Yu H, Zhou W, Silberstein LE, Cheng T, Han M, Xu Y, Luo HR, Gasdermin D Exerts Anti-inflammatory Effects by Promoting Neutrophil Death. Cell reports 22, 2924–2936 (2018). [PubMed: 29539421]

19. Sarhan J, Liu BC, Muendlein HI, Li P, Nilson R, Tang AY, Rongvaux A, Bunnell SC, Shao F, Green DR, Poltorak A, Caspase-8 induces cleavage of gasdermin D to elicit pyroptosis during Yersinia infection. Proc Natl Acad Sci U S A 115, E10888–E10897 (2018). [PubMed: 30381458]

20. Burgener SS, Leborgne NGF, Snipas SJ, Salvesen GS, Bird PI, Benarafa C, Cathepsin G Inhibition by Serpinb1 and Serpinb6 Prevents Programmed Necrosis in Neutrophils and Monocytes and Reduces GSDMD-Driven Inflammation. Cell reports 27, 3646–3656 e3645 (2019). [PubMed: 31216481]

21. Evavold CL, Ruan J, Tan Y, Xia S, Wu H, Kagan JC, The Pore-Forming Protein Gasdermin D Regulates Interleukin-1 Secretion from Living Macrophages. Immunity 48, 35–44 e36 (2018). [PubMed: 29195811]

22. Humphries F, Shmuel-Galia L, Ketelut-Carneiro N, Li S, Wang B, Nemmara VV, Wilson R, Jiang Z, Khalighinejad F, Muneeruddin K, Shaffer SA, Dutta R, Ionete C, Pesiridis S, Yang S, Thompson PR, Fitzgerald KA, Succination inactivates gasdermin D and blocks pyroptosis. Science 369, 1633–1637 (2020). [PubMed: 32820063]

23. Evavold CL, Hafner-Bratkovic I, Devant P, D'Andrea JM, Ngwa EM, Borsic E, Doench JG, LaFleur MW, Sharpe AH, Thiagarajah JR, Kagan JC, Control of gasdermin D oligomerization and pyroptosis by the Ragulator-Rag-mTORC1 pathway. Cell 184, 4495–4511 e4419 (2021). [PubMed: 34289345]

24. Kayagaki N, Kornfeld OS, Lee BL, Stowe IB, O'Rourke K, Li Q, Sandoval W, Yan D, Kang J, Xu M, Zhang J, Lee WP, McKenzie BS, Ulas G, Payandeh J, Roose-Girma M, Modrusan Z, Reja R, Sagolla M, Webster JD, Cho V, Andrews TD, Morris LX, Miosge LA, Goodnow CC, Bertram EM,

Dixit VM, NINJ1 mediates plasma membrane rupture during lytic cell death. Nature 591, 131–136 (2021). [PubMed: 33472215]

25. Kayagaki N, Stowe IB, Alegre K, Deshpande I, Wu S, Lin Z, Kornfeld OS, Lee BL, Zhang J, Liu J, Suto E, Lee WP, Schneider K, Lin W, Seshasayee D, Bhangale T, Chalouni C, Johnson MC, Joshi P, Mossemann J, Zhao S, Ali D, Goldenberg NM, Sayed BA, Steinberg BE, Newton K, Webster JD, Kelly RL, Dixit VM, Inhibiting membrane rupture with NINJ1 antibodies limits tissue injury. Nature 618, 1072–1077 (2023). [PubMed: 37196676]
26. Degen M, Santos JC, Pluhackova K, Cebrero G, Ramos S, Jankevicius G, Hartenian E, Guillerm U, Mari SA, Kohl B, Müller DJ, Schanda P, Maier T, Perez C, Sieben C, Broz P, Hiller S, Structural basis of NINJ1-mediated plasma membrane rupture in cell death. Nature 618, 1065–1071 (2023). [PubMed: 37198476]
27. Santa Cruz Garcia AB, Schnur KP, Malik AB, Mo GCH, Gasdermin D pores are dynamically regulated by local phosphoinositide circuitry. Nature communications 13, 52 (2022).
28. Fiorentino M, Zadra G, Palescandolo E, Fedele G, Bailey D, Fiore C, Nguyen PL, Migita T, Zamponi R, Di Vizio D, Priolo C, Sharma C, Xie W, Hemler ME, Mucci L, Giovannucci E, Finn S, Loda M, Overexpression of fatty acid synthase is associated with palmitoylation of Wnt1 and cytoplasmic stabilization of beta-catenin in prostate cancer. Lab Invest 88, 1340–1348 (2008). [PubMed: 18838960]
29. Wei X, Schneider JG, Shenouda SM, Lee A, Towler DA, Chakravarthy MV, Vita JA, Semenkovich CF, De novo lipogenesis maintains vascular homeostasis through endothelial nitric-oxide synthase (eNOS) palmitoylation. J Biol Chem 286, 2933–2945 (2011). [PubMed: 21098489]
30. Wei X, Yang Z, Rey FE, Ridaura VK, Davidson NO, Gordon JI, Semenkovich CF, Fatty acid synthase modulates intestinal barrier function through palmitoylation of mucin 2. Cell Host Microbe 11, 140–152 (2012). [PubMed: 22341463]
31. Kim YC, Lee SE, Kim SK, Jang HD, Hwang I, Jin S, Hong EB, Jang KS, Kim HS, Toll-like receptor mediated inflammation requires FASN-dependent MYD88 palmitoylation. Nat Chem Biol 15, 907–916 (2019). [PubMed: 31427815]
32. Di Vizio D, Adam RM, Kim J, Kim R, Sotgia F, Williams T, Demichelis F, Solomon KR, Loda M, Rubin MA, Lisanti MP, Freeman MR, Caveolin-1 interacts with a lipid raft-associated population of fatty acid synthase. Cell Cycle 7, 2257–2267 (2008). [PubMed: 18635971]
33. Bollu LR, Ren J, Blessing AM, Katreddy RR, Gao G, Xu L, Wang J, Su F, Weihua Z, Involvement of de novo synthesized palmitate and mitochondrial EGFR in EGF induced mitochondrial fusion of cancer cells. Cell Cycle 13, 2415–2430 (2014). [PubMed: 25483192]
34. Du G, Healy LB, David L, Walker C, Fontana P, Dong Y, Devant P, Puthenveetil R, Ficarro SB, Banerjee A, Kagan JC, Lieberman J, Wu H, ROS-dependent palmitoylation is an obligate licensing modification for GSDMD pore formation. bioRxiv, 2023.2003.2007.531538 (2023).
35. Hu L, Chen M, Chen X, Zhao C, Fang Z, Wang H, Dai H, Chemotherapy-induced pyroptosis is mediated by BAK/BAX-caspase-3-GSDME pathway and inhibited by 2-bromopalmitate. Cell Death Dis 11, 281 (2020). [PubMed: 32332857]
36. Zheng B, Zhu S, Wu X, Clickable analogue of cerulenin as chemical probe to explore protein palmitoylation. ACS Chem Biol 10, 115–121 (2015). [PubMed: 25322207]
37. Jennings BC, Nadolski MJ, Ling Y, Baker MB, Harrison ML, Deschenes RJ, Linder ME, 2-Bromopalmitate and 2-(2-hydroxy-5-nitro-benzylidene)-benzo[b]thiophen-3-one inhibit DHHC-mediated palmitoylation in vitro. J Lipid Res 50, 233–242 (2009). [PubMed: 18827284]
38. Abrami L, Audagnotto M, Ho S, Marcaida MJ, Mesquita FS, Anwar MU, Sandoz PA, Fonti G, Pojer F, Dal Peraro M, van der Goot FG, Palmitoylated acyl protein thioesterase APT2 deforms membranes to extract substrate acyl chains. Nat Chem Biol 17, 438–447 (2021). [PubMed: 33707782]
39. Moon JS, Lee S, Park MA, Siempos II, Haslip M, Lee PJ, Yun M, Kim CK, Howrylak J, Ryter SW, Nakahira K, Choi AM, UCP2-induced fatty acid synthase promotes NLRP3 inflammasome activation during sepsis. J Clin Invest 125, 665–680 (2015). [PubMed: 25574840]
40. Wang L, Cai J, Zhao X, Ma L, Zeng P, Zhou L, Liu Y, Yang S, Cai Z, Zhang S, Zhou L, Yang J, Liu T, Jin S, Cui J, Palmitoylation prevents sustained inflammation by limiting

NLRP3 inflammasome activation through chaperone-mediated autophagy. Molecular Cell 83, 281–297.e210 (2023). [PubMed: 36586411]

41. Devant P, Boršić E, Ngwa EM, Xiao H, Chouchani ET, Thiagarajah JR, Hafner-Bratkovič I, Evavold CL, Kagan JC, Gasdermin D pore-forming activity is redox-sensitive. Cell reports 42, 112008 (2023). [PubMed: 36662620]
42. Martin BR, Cravatt BF, Large-scale profiling of protein palmitoylation in mammalian cells. Nat Methods 6, 135–138 (2009). [PubMed: 19137006]
43. Bolhassani A, Jafarzade BS, Mardani G, In vitro and in vivo delivery of therapeutic proteins using cell penetrating peptides. Peptides 87, 50–63 (2017). [PubMed: 27887988]
44. Liang L, Wang H, Shi H, Li Z, Yao H, Bu Z, Song N, Li C, Xiang D, Zhang Y, Wang J, Hu Y, Xu Q, Ma Y, Cheng Z, Wang Y, Zhao S, Qian J, Chen Y, Fang JY, Xu J, A Designed Peptide Targets Two Types of Modifications of p53 with Anti-cancer Activity. Cell chemical biology 25, 761–774 e765 (2018). [PubMed: 29681526]
45. Soragni A, Janzen DM, Johnson LM, Lindgren AG, Thai-Quynh Nguyen A, Tiourin E, Soriaga AB, Lu J, Jiang L, Faull KF, Pellegrini M, Memarzadeh S, Eisenberg DS, A Designed Inhibitor of p53 Aggregation Rescues p53 Tumor Suppression in Ovarian Carcinomas. Cancer Cell 29, 90–103 (2016). [PubMed: 26748848]
46. Yao H, Lan J, Li C, Shi H, Brosseau J-P, Wang H, Lu H, Fang C, Zhang Y, Liang L, Zhou X, Wang C, Xue Y, Cui Y, Xu J, Inhibiting PD-L1 palmitoylation enhances T-cell immune responses against tumours. Nature Biomedical Engineering 3, 306–317 (2019).
47. Yao H, Li C, He F, Song T, Brosseau JP, Wang H, Lu H, Fang C, Shi H, Lan J, Fang JY, Xu J, A peptidic inhibitor for PD-1 palmitoylation targets its expression and functions. RSC Chem Biol 2, 192–205 (2021). [PubMed: 34458782]
48. Skotte NH, Sanders SS, Singaraja RR, Ehrnhoefer DE, Vaid K, Qiu X, Kannan S, Verma C, Hayden MR, Palmitoylation of caspase-6 by HIP14 regulates its activation. Cell Death & Differentiation 24, 433–444 (2017).
49. Turnbull AP, Kümmel D, Prinz B, Holz C, Schultchen J, Lang C, Niesen FH, Hofmann KP, Delbrück H, Behlke J, Müller EC, Jarosch E, Sommer T, Heinemann U, Structure of palmitoylated BET3: insights into TRAPP complex assembly and membrane localization. Embo j 24, 875–884 (2005). [PubMed: 15692564]
50. Johnson AG, Wein T, Mayer ML, Duncan-Lowey B, Yirmiya E, Oppenheimer-Shaanan Y, Amitai G, Sorek R, Kranzusch PJ, Bacterial gasdermins reveal an ancient mechanism of cell death. Science 375, 221–225 (2022). [PubMed: 35025633]
51. Greaves J, Chamberlain LH, DHHC palmitoyl transferases: substrate interactions and (patho)physiology. Trends Biochem Sci 36, 245–253 (2011). [PubMed: 21388813]
52. Sobocinska J, Roszczenko-Jasinska P, Zareba-Koziol M, Hromada-Judycka A, Matveichuk OV, Traczyk G, Lukasiuk K, Kwiatkowska K, Lipopolysaccharide Upregulates Palmitoylated Enzymes of the Phosphatidylinositol Cycle: An Insight from Proteomic Studies. Mol Cell Proteomics 17, 233–254 (2018). [PubMed: 29217618]
53. Geng S, Chen K, Yuan R, Peng L, Maitra U, Diao N, Chen C, Zhang Y, Hu Y, Qi C-F, Pierce S, Ling W, Xiong H, Li L, The persistence of low-grade inflammatory monocytes contributes to aggravated atherosclerosis. Nature communications 7, 13436 (2016).
54. Yuan R, Geng S, Li L, Molecular Mechanisms That Underlie the Dynamic Adaptation of Innate Monocyte Memory to Varying Stimulant Strength of TLR Ligands. Frontiers in immunology 7, 497 (2016). [PubMed: 27891130]
55. Ding X, Kambara H, Guo R, Kanneganti A, Acosta-Zaldivar M, Li J, Liu F, Bei T, Qi W, Xie X, Han W, Liu N, Zhang C, Zhang X, Yu H, Zhao L, Ma F, Kohler JR, Luo HR, Inflammasome-mediated GSDMD activation facilitates escape of Candida albicans from macrophages. Nature communications 12, 6699 (2021).
56. Rathkey JK, Zhao J, Liu Z, Chen Y, Yang J, Kondolf HC, Benson BL, Chirieleison SM, Huang AY, Dubyak GR, Xiao TS, Li X, Abbott DW, Chemical disruption of the pyroptotic pore-forming protein gasdermin D inhibits inflammatory cell death and sepsis. Science immunology 3, (2018).
57. Hu JJ, Liu X, Xia S, Zhang Z, Zhang Y, Zhao J, Ruan J, Luo X, Lou X, Bai Y, Wang J, Hollingsworth LR, Magupalli VG, Zhao L, Luo HR, Kim J, Lieberman J, Wu H, FDA-approved

disulfiram inhibits pyroptosis by blocking gasdermin D pore formation. Nat Immunol 21, 736–745 (2020). [PubMed: 32367036]

58. Fritsch J, Särchen V, Schneider-Brachert W, Regulation of Death Receptor Signaling by S-Palmitoylation and Detergent-Resistant Membrane Micro Domains—Greasing the Gears of Extrinsic Cell Death Induction, Survival, and Inflammation. Cancers 13, 2513 (2021). [PubMed: 34063813]
59. Fukata Y, Fukata M, Protein palmitoylation in neuronal development and synaptic plasticity. Nature reviews. Neuroscience 11, 161–175 (2010). [PubMed: 20168314]
60. Resh MD, Palmitoylation of proteins in cancer. Biochem Soc Trans 45, 409–416 (2017). [PubMed: 28408481]
61. Fukata Y, Murakami T, Yokoi N, Fukata M, Local Palmitoylation Cycles and Specialized Membrane Domain Organization. Current topics in membranes 77, 97–141 (2016). [PubMed: 26781831]
62. Weindel CG, Martinez EL, Zhao X, Mabry CJ, Bell SL, Vail KJ, Coleman AK, VanPortfliet JJ, Zhao B, Wagner AR, Azam S, Scott HM, Li P, West AP, Karpac J, Patrick KL, Watson RO, Mitochondrial ROS promotes susceptibility to infection via gasdermin D-mediated necroptosis. Cell 185, 3214–3231.e3223 (2022). [PubMed: 35907404]
63. Miao R, Jiang C, Chang WY, Zhang H, An J, Ho F, Chen P, Zhang H, Junqueira C, Amgalan D, Liang FG, Zhang J, Evavold CL, Hafner-Bratkovič I, Zhang Z, Fontana P, Xia S, Waldeck-Weiermair M, Pan Y, Michel T, Bar-Peled L, Wu H, Kagan JC, Kitsis RN, Zhang P, Liu X, Lieberman J, Gasdermin D permeabilization of mitochondrial inner and outer membranes accelerates and enhances pyroptosis. Immunity, (2023).
64. Rittirsch D, Huber-Lang MS, Flierl MA, Ward PA, Immunodesign of experimental sepsis by cecal ligation and puncture. Nature protocols 4, 31–36 (2009). [PubMed: 19131954]
65. Yang X, Cheng X, Tang Y, Qiu X, Wang Y, Kang H, Wu J, Wang Z, Liu Y, Chen F, Xiao X, Mackman N, Billiar TR, Han J, Lu B, Bacterial Endotoxin Activates the Coagulation Cascade through Gasdermin D-Dependent Phosphatidylserine Exposure. Immunity 51, 983–996 e986 (2019). [PubMed: 31836429]
66. Waterhouse A, Bertoni M, Bienert S, Studer G, Tauriello G, Gumienny R, Heer FT, de Beer TAP, Rempfer C, Bordoli L, Lepore R, Schwede T, SWISS-MODEL: homology modelling of protein structures and complexes. Nucleic Acids Res 46, W296–W303 (2018). [PubMed: 29788355]
67. Xie X, Shi Q, Wu P, Zhang X, Kambara H, Su J, Yu H, Park SY, Guo R, Ren Q, Zhang S, Xu Y, Silberstein LE, Cheng T, Ma F, Li C, Luo HR, Single-cell transcriptome profiling reveals neutrophil heterogeneity in homeostasis and infection. Nat Immunol 21, 1119–1133 (2020). [PubMed: 32719519]

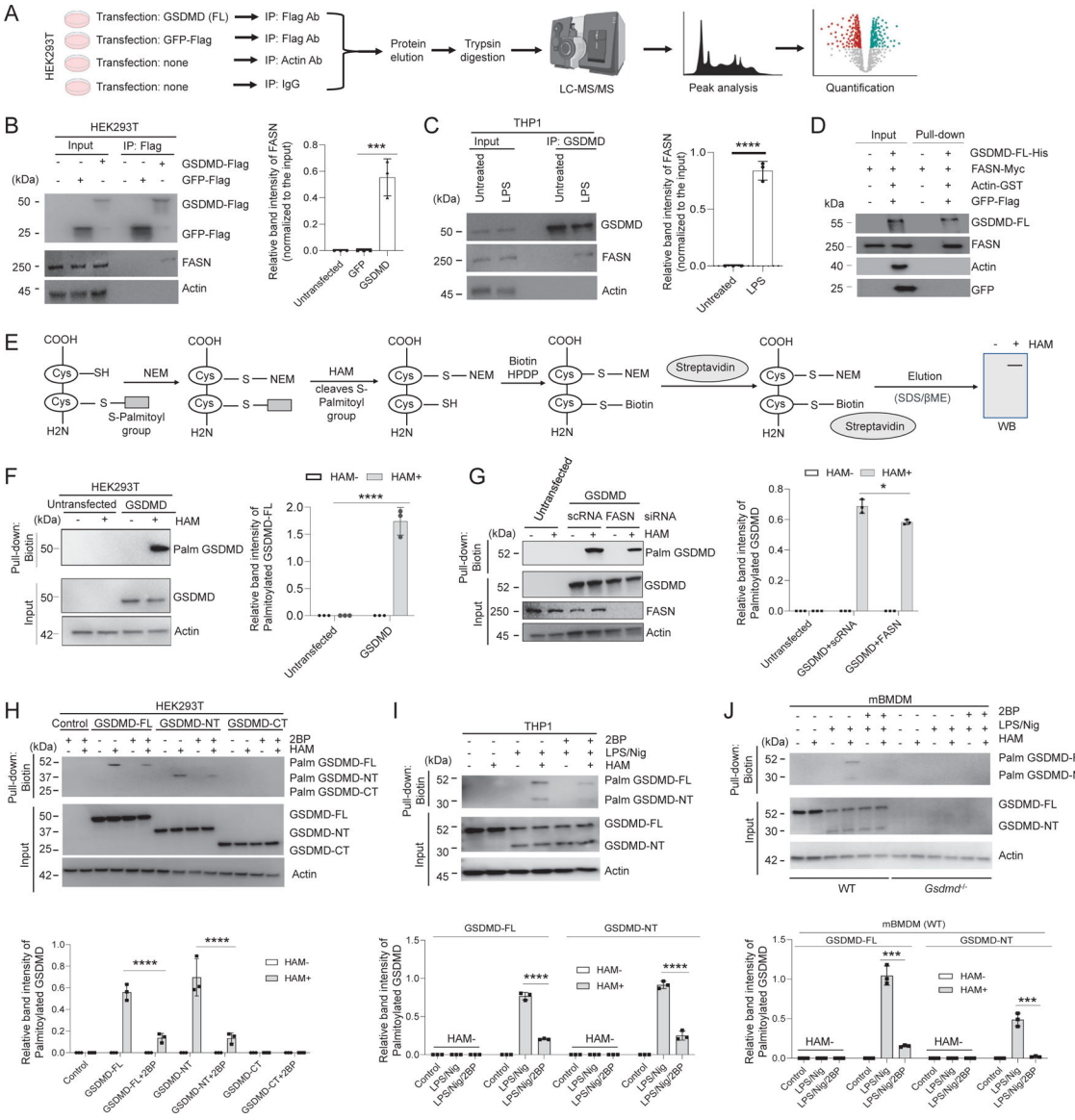

Fig. 1. GSDMD interacts with FASN and both full-length (GSDMD-FL) and cleaved GSDMD-NT are palmitoylated.

(**A**) Schematic of the approach and strategy used to identify GSDMD-interacting proteins by mass spectrometry. (**B**) FASN-GSDMD interaction in HEK293T cells expressing hGSDMD-FL-FLAG. Right: quantification of relative FASN protein bound with GSDMD-FL. n=3 biological replicates. (**C**) FASN–GSDMD interaction in PMA-differentiated THP-1. Right: quantification of endogenous FASN bound with GSDMD protein. n=3 biological replicates. (**D**) Interaction between c-Myc-tagged FASN and His-tagged hGSDMD-FL. Immunoblot analyses were performed using anti-GSDMD and other indicated antibodies. n=3 biological replicates. (**E**) Schematic of the steps in the acyl-biotin exchange (ABE) palmitoylation assay. (**F**) GSDMD palmitoylation in HEK293T cells. n=3 biologically independent experiments. (**G**) FLAG-hGSDMD-FL was coexpressed with control or *FASN* siRNA and subjected to the ABE palmitoylation assay and immunoblot analyses. n=3 biological replicates. (**H**) Palmitoylation of GSDMD-FL, GSDMD-N, or GSDMD-C in the presence or

absence of 2BP. n=3 biological replicates. (**I**) GSDMD palmitoylation in PMA-differentiated macrophage-like THP-1 cells. Cells were treated with or without LPS for 3 hours, followed by 2BP treatment for 30 min and then nigericin treatment for 35 min. Immunoblot analyses were performed with anti-GSDMD antibodies. n=3 biological replicates. (**J**) GSDMD palmitoylation in primary mouse bone marrow-derived macrophages (mBMDM). Cells were cultured in the presence of LPS (1 μg/ml) (3 hours), followed by 2BP 10 μM (30 min) and treatment with nigericin (20 μM) for 1 hour. n=3 biological replicates. (B, C, F, G, H, I, and J) Data are mean ± SEM. Immunoblots shown are representative of three independent experiments. *P<0.05, **P<0.01, ***P<0.001, ****P<0.0001. Statistical analyses were performed using one-way ANOVA with Bonferroni's multiple comparison test (B), unpaired Student's t test (C), or two-way ANOVA with Bonferroni's multiple comparison test (F-J).

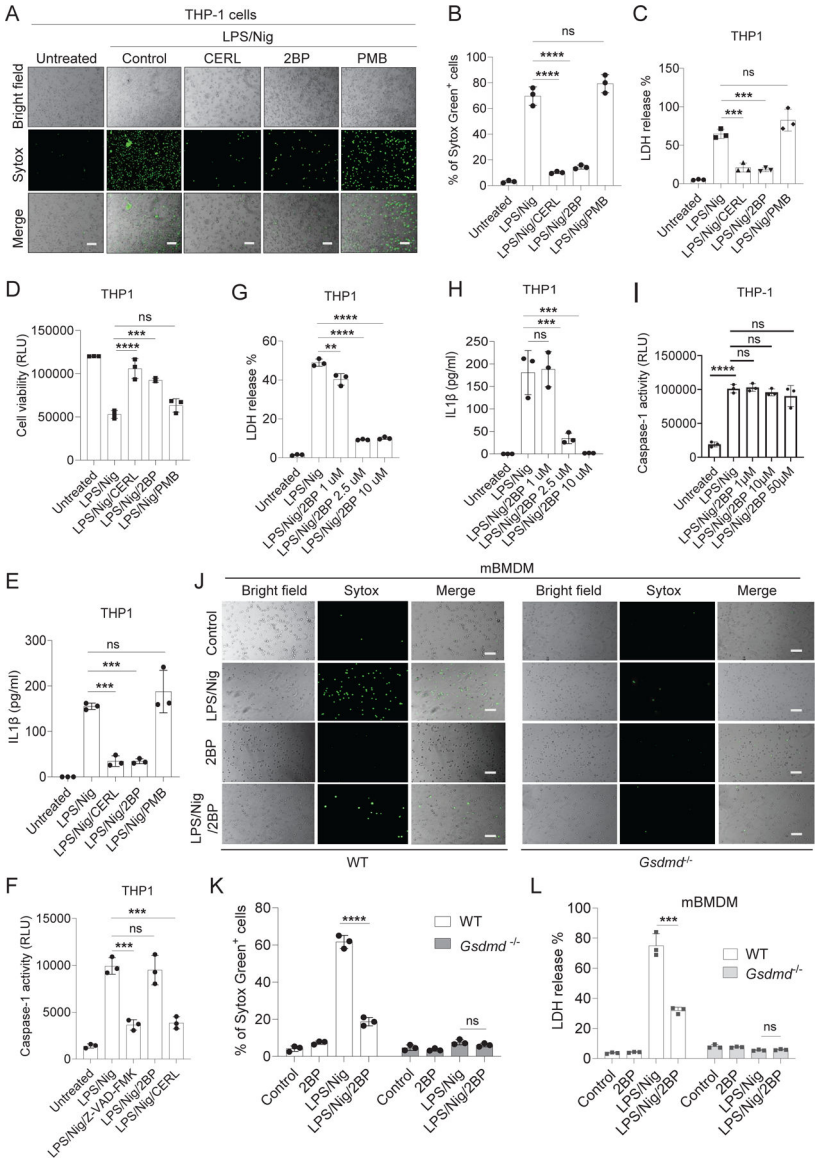

Fig. 2. Inhibition of palmitoylation impairs pyroptosis in macrophages.

(**A**) Representative brightfield and fluorescence images of THP-1 cells primed with LPS (3 hours) followed by treatment with palmitoylation inhibitors (cerulenin, 50 μM; 2-bromopalmitate, 10 μM) and depalmitoylation inhibitor (palmostatin B, 50 μM) for 30 min before stimulation with nigericin for 35 min. Pyroptotic pore formation was assessed with the SYTOX Green dye binding assay using ImageJ software. Scale bars: 100 μm. n=3 biological replicates. (**B**) Quantification of relative SYTOX uptake in THP-1 cells. (**C**) LDH release from THP-1 cells. n=3 biological replicates. (**D**) Relative cell viability was calculated using the RealTime-Glo MT Cell Viability Assay. n=3 biological replicates. (**E**) IL-1β secretion by THP-1 cells was measured by ELISA. n=3 biological replicates. (**F**) The relative abundance of active caspase in THP-1 cell culture supernatants was quantified with Caspase-1 Glo reagent (Promega). n=3 biological replicates. (**G**) THP-1 cells treated with or without LPS/Nig in the presence or absence of 2BP were treated at different concentrations.

The resulting supernatants were quantified for LDH release. n=3 biological replicates. (**H**) IL-1β release from THP-1 cells. n=3 biological replicates. (**I**) The effect of 2BP treatment on caspase-1 activity. n=3 biological replicates. (**J**) mBMDM from WT and *Gsdmd*$^{-/-}$ mice were primed with or without LPS for 3 hours in the presence or absence of 2BP for 30 min before stimulation with nigericin for 1 hour. Pyroptotic pore formation was assessed with the SYTOX Green assay, and fluorescence images were captured and quantified using ImageJ. Scale bars: 100 μm. n=3 biological replicates. (**K**) Quantification of relative SYTOX uptake in mBMDMs. (**L**) LDH release from WT and *Gsdmd*$^{-/-}$ cell. n=3 biological replicates. (B to L) All data are representative of three independent experiments. Data are means ± SEM. ***P*<0.01, ****P*<0.001, ****P<0.0001. Statistical analyses were performed using one-way (B to I) or two-way (K and L) ANOVA with Bonferroni's multiple comparison test.

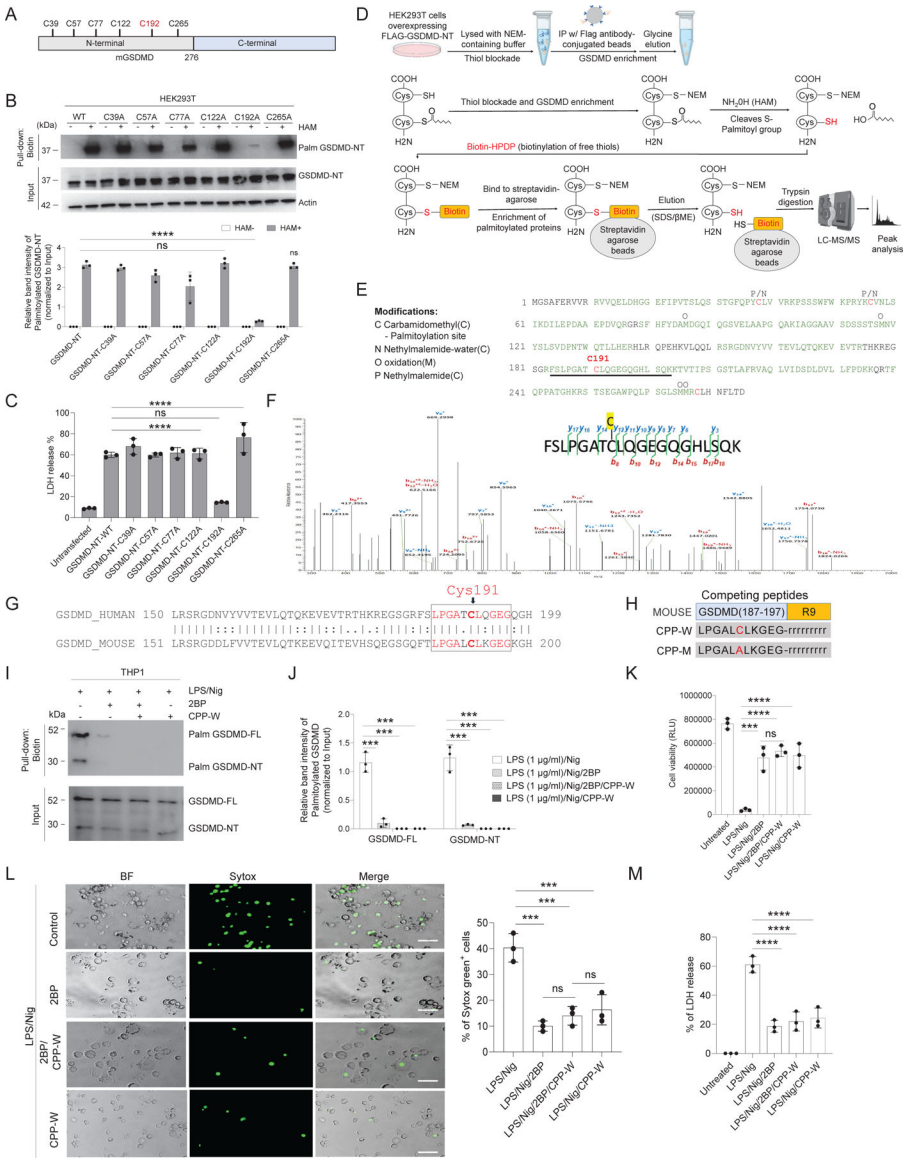

Fig. 3. GSDMD palmitoylation occurs on Cys192.

(**A**) A schematic of the number of cysteine residues present in mouse GSDMD-NT. Highlighted in red is a potential cysteine site in GSDMD-NT that is palmitoylated. (**B**) Palmitoylation of WT GSDMD-NT or mutant GSDMD-NT (Cys39A, Cys57A, Cys77A, Cys122A, Cys192A, Cys265A) in HEK293T cells. Immunoblot analyses were performed with anti-FLAG HRP antibody. Palmitoylated proteins were quantified and normalized to corresponding input. n=3 biological replicates. (**C**) LDH release. n=3 biological replicates. (**D**) Schematic of the approach and strategy used to identify GSDMD palmitoylation by mass spectrometry. (**E**) Posttranslational modifications identified in GSDMD-NT protein. Protein sequences covered by MS analyses are marked in green. (**F**) MS/MS CID fragmentation spectrum of the peptide FSLPGATCLQGEGQGHLSQK (m/z 1058.02013, $[M+2H]^{2+}$) containing carbamidomethylation at C8 (Cys192). (**G** to **M**) A competitive peptide, CPP-W, specifically inhibits GSDMD palmitoylation and suppresses macrophage

pyroptosis. (G) Protein sequence alignment of human and mouse GSDMD using EMBOSS Matcher. (H) Cell-permeable, GSDMD-competing peptides. R9 represents poly-arginine. Lower case amino acid symbol (r) represents the D-form of arginine. (I) GSDMD palmitoylation in PMA differentiated THP-1 cells primed with LPS (1 μg/ml) for 2 hours at 37°C, followed by 2BP (50 μM) or 2BP plus CPP-W (50 μM) treatment for 30 min. Nigericin (10 μM, 30 min) was then added to trigger inflammasome activation. n=3 biological replicates. (J) Quantification of palmitoylated GSDMD normalized to input. (K) Relative cell viability was calculated using the RealTime-Glo MT Cell Viability Assay. n=3 biological replicates. (L) Pyroptotic pore formation was assessed with the SYTOX Green assay, and fluorescence images were captured and quantified using ImageJ. Scale bars: 50 μm. n=3 biological replicates. (M) LDH release. n=3 biological replicates. (B, C, J, K, L, and M) All data are representative of three independent experiments. Data are means ± SEM. $^{**}P<0.01$, $^{***}P<0.001$, ****P<0.0001. Statistical analyses were performed using one-way (C, K, L, and M) or two-way (B and J) ANOVA with Bonferroni's multiple comparison test.

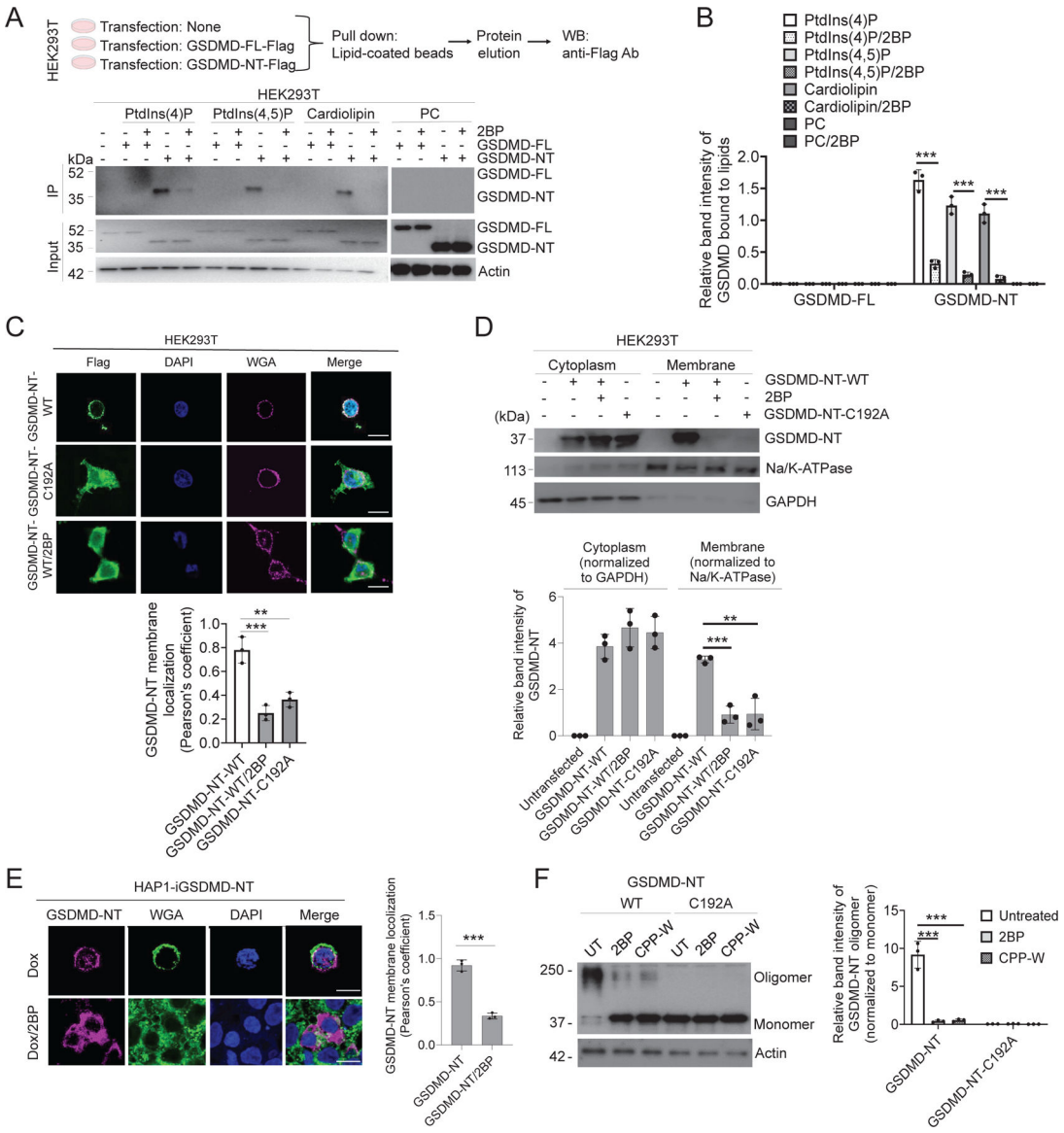

Fig. 4. Palmitoylation of GSDMD-NT is required for its membrane translocation and oligomerization.

(**A**) Schematic approach and strategy used to detect GSDMD-lipid binding. HEK293T cells were transfected with either human GSDMD-FL-FLAG or GSDMD-NT-FLAG and cultured for 24 hours in the presence or absence of 2BP (50 μM). Following cell lysis, the lysates were co-precipitated with agarose beads coated with specific lipids. Immunoblot analyses were subsequently performed using anti-FLAG HRP antibodies. n=3 biological replicates. (**B**) Quantification of the relative amount of GSDMD bound to the lipid-coated beads. n=3 biological replicates. (**C**) Representative Subcellular localization of GSDMD-NT in HEK293T cells. Scale bars: 10 μm. Green: GSDMD; blue: nuclei (DAPI); and magenta: plasma membrane (wheat germ agglutinin (WGA). Results are presented as normalized Pearson's correlation. At least 20 cells were randomly picked and analyzed for each sample. n=3 biological replicates. (**D**) Distribution of GSDMD-NT and mutant in subcellular fractions of HEK293T cells subjected to immunoblot analysis. n=3 biological replicates.

(**E**) Subcellular localization of GSDMD-NT in Dox-induced GSDMD-NT cells treated with or without 2BP. Scale bars: 10 μm. Green: GSDMD; magenta: plasma membrane (WGA); and blue: nuclei (DAPI). Images shown are representative of at least ten random fields from three independent experiments. n=3 biological replicates. (**F**) Inhibition of palmitoylation impaired GSDMD oligomerization. Right: quantification of relative oligomer normalized with monomer. n=3 biological replicates. (B to F) All data are representative of three independent experiments. Data are mean ± SEM. $^{**}P<0.01$, $^{***}P<0.001$. Statistical analyses were performed using one-way ANOVA with Bonferroni's multiple comparison test (C and D), unpaired Student's *t* test (E), or two-way ANOVA with Bonferroni's multiple comparison test (B and F).

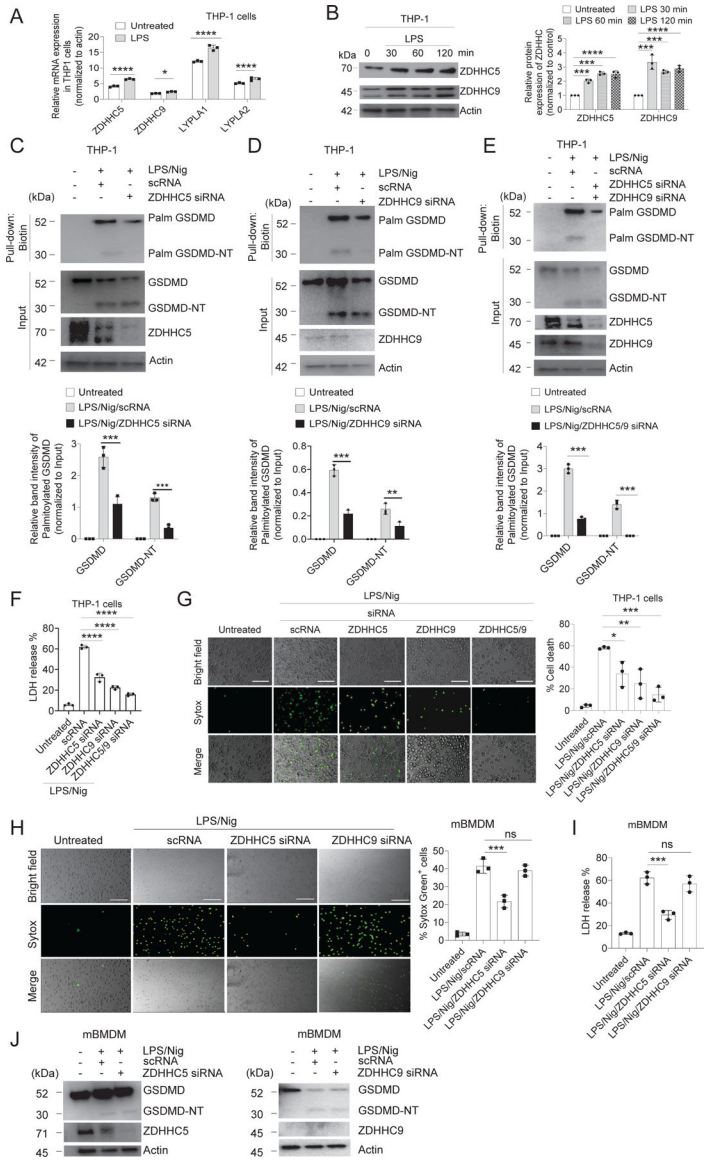

Fig. 5. ZDHHC5 and ZDHHC9-mediated palmitoylation is required for LPS/Nig-triggered pyroptosis in macrophages.

(**A**) Expression of palmitoylation-related genes in THP-1 cells. Real-time PCR analysis was conducted using THP-1 cells primed with LPS for 3 hours. mRNA expression of *ZDHHC* was quantified and normalized to actin. n=3 biological replicates. (**B**) LPS-induced expression of ZDHHC5 and ZDHHC9 protein in THP-1 cells. PMA differentiated THP-1 cells were treated with LPS (100 ng/ml) for indicated time. Right, quantification of relative expression of ZDHHC protein using ImageJ. n=3 biological replicates. (**C** to **E**) THP-1 cells were transiently transfected with control or siRNA targeting (C) *ZDHHC5*, (D) *ZDHHC9*, and (E) *ZDHHC5/9* followed by priming with LPS for 3 hours and treatment with nigericin for 35 min. The ABE assay and immunoblot analysis were then performed with anti-GSDMD antibodies. Bar graph depicts the quantification of palmitoylated GSDMD protein normalized to relative input. n=3 biological replicates. (**F**) LDH release. n=3 biological replicates. (**G**) Fluorescence images of SYTOX Green uptake in THP-1 cells expressing

control and *ZDHHC* siRNA. Scale bars: 100 μm. Right: quantification of relative SYTOX uptake in THP-1 cells. n=3 biological replicates. (**H** to **J**) ZDHHC5 palmitoyl enzyme mediates pyroptotic cell death in primary mouse macrophages. (H) Fluorescence images of SYTOX Green uptake in mBMDMs transfected with control or *ZDHHC* siRNA. Scale bars: 100 μm. Right, quantification of SYTOX uptake. n=3 biological replicates. (I) LDH release from mBMDMs. n=3 biological replicates. (J) mBMDMs transfected with control or *Zdhhc* siRNAs were treated with or without LPS/Nig. Cells were lysed and subjected to immunoblot analysis. Immunoblot images are representative of three independent repeats. n=3 biological replicates. (A to H) All data are representative of three independent experiments. Data are mean ± SEM. **P*<0.05, ***P*<0.01, ****P*<0.001, **** *P*<0.0001. Statistical analyses were performed using one-way (F to H) or two-way (A to E) ANOVA with Bonferroni's multiple comparison test.

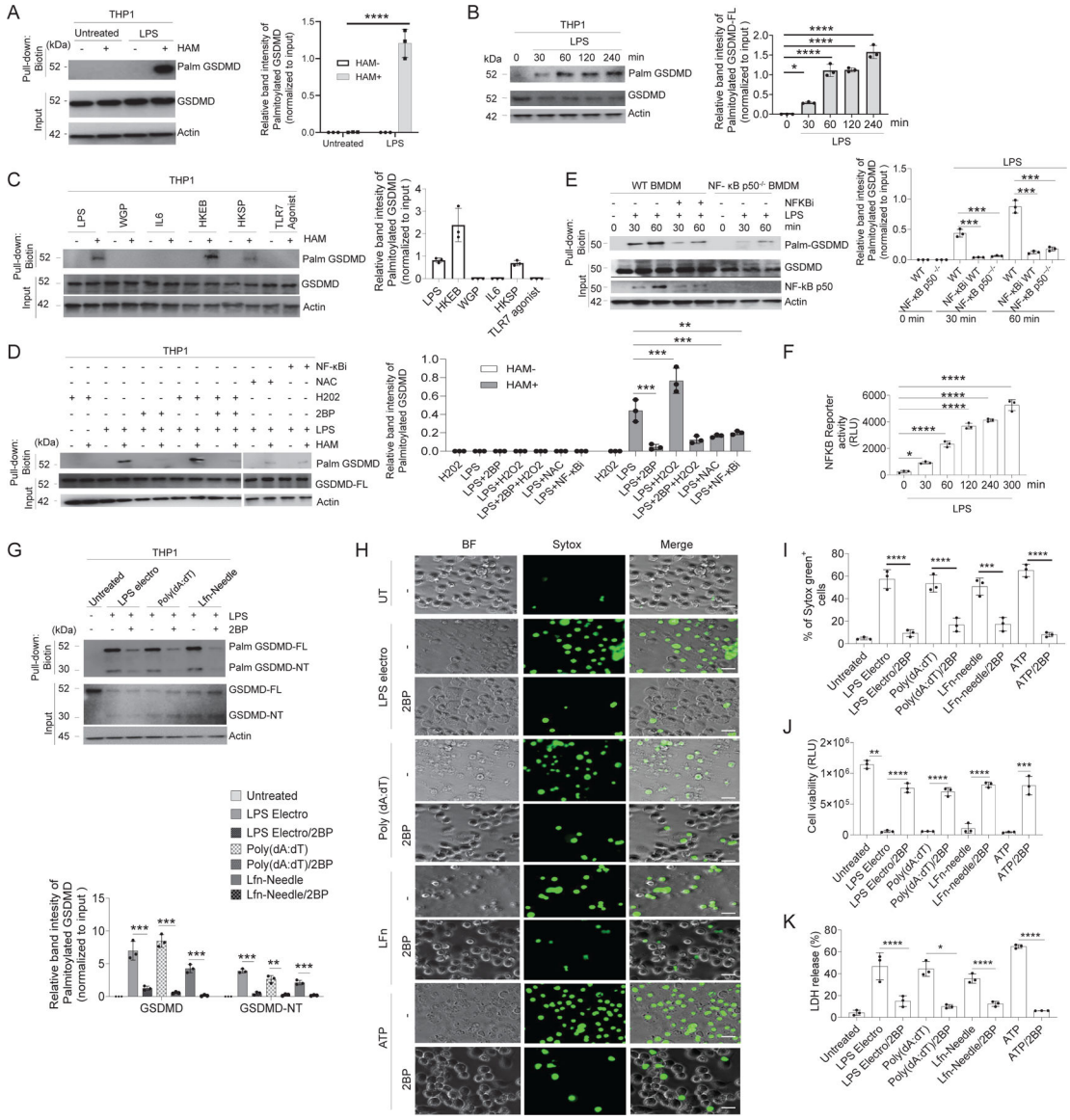

Fig. 6. GSDMD palmitoylation is tightly regulated.

(**A**) GSDMD palmitoylation in PMA differentiated THP-1 cells stimulated with LPS (100 ng/ml) for 2 hours. n=3 biological replicates. (**B**) Time course of LPS-induced GSDMD palmitoylation. n=3 biological replicates. (**C**) GSDMD palmitoylation in PMA-differentiated THP-1 cells stimulated with LPS (1 μg/ml), whole glucan particles (WGP) (100 μg/ml), IL-6 (600 pg/ml), heat-killed *E. coli* (HKEB) (10^5 cells/ml), heat-killed *S. pneumonia* (HKSP) (10^7 cells/ml), or a TLR7 agonist (imidazoquinoline) (2.5 μg/ml) for 2 hours at 37°C. n=3 biological replicates. (**D**) GSDMD palmitoylation in PMA-differentiated THP-1 cells treated with or without LPS for 3 hours in the presence or absence of H_2O_2 (625 μM), 2BP (10 μM), NAC (3 mM), or JSH-23 (NF-κBi) (50 μM). n=3 biological replicates. (**E**) GSDMD palmitoylation in mouse primary bone marrow-derived WT and NF-κB *p50*$^{-/-}$ macrophages treated with LPS (100 ng/ml) in the presence or absence of NF-κBi (20 μM). n=3 biological replicates. (**F**) Time course of LPS-induced of NF-κB activation in PMA

differentiated THP-1-NF-κB-Luc cells. n=3 biological replicates. (**G** to **K**) 2BP suppresses macrophage pyroptosis triggered by various inflammasomes. PMA-differentiated THP-1 cells were primed with LPS (1 μg/ml) for 2 hours at 37°C. The AIM2 inflammasome was activated using precomplexed Poly(dA:dT)/LyoVec™ (1 μg/ml) and NLRC4/NAIP inflammasome was activated using Lfn-Needle (Needle-Tox) (4 ng/ml). Non-canonical inflammasome (caspase-11) activation was induced by LPS electroporation (1 μg/ml). All subsequent assays were conducted 24 hours thereafter. (G) GSDMD palmitoylation. n=3 biological replicates. (H) Pyroptotic pore formation assessed with the SYTOX Green assay. Scale bars: 50 μM. n=3 biological replicates. (I) Quantification of relative SYTOX uptake. n=3 biological replicates. (J) Relative cell viability calculated using the RealTime-Glo MT Cell Viability Assay. n=3 biological replicates. (K) LDH release. n=3 biological replicates. (A to K) All data are representative of three independent experiments. Data are mean ± SEM. *P<0.05, **P<0.01, ***P<0.001, **** P<0.0001. Statistical analyses were performed using one-way (B, E, F, and I to K) or two-way (A, D, and G) ANOVA with Bonferroni's multiple comparison test.

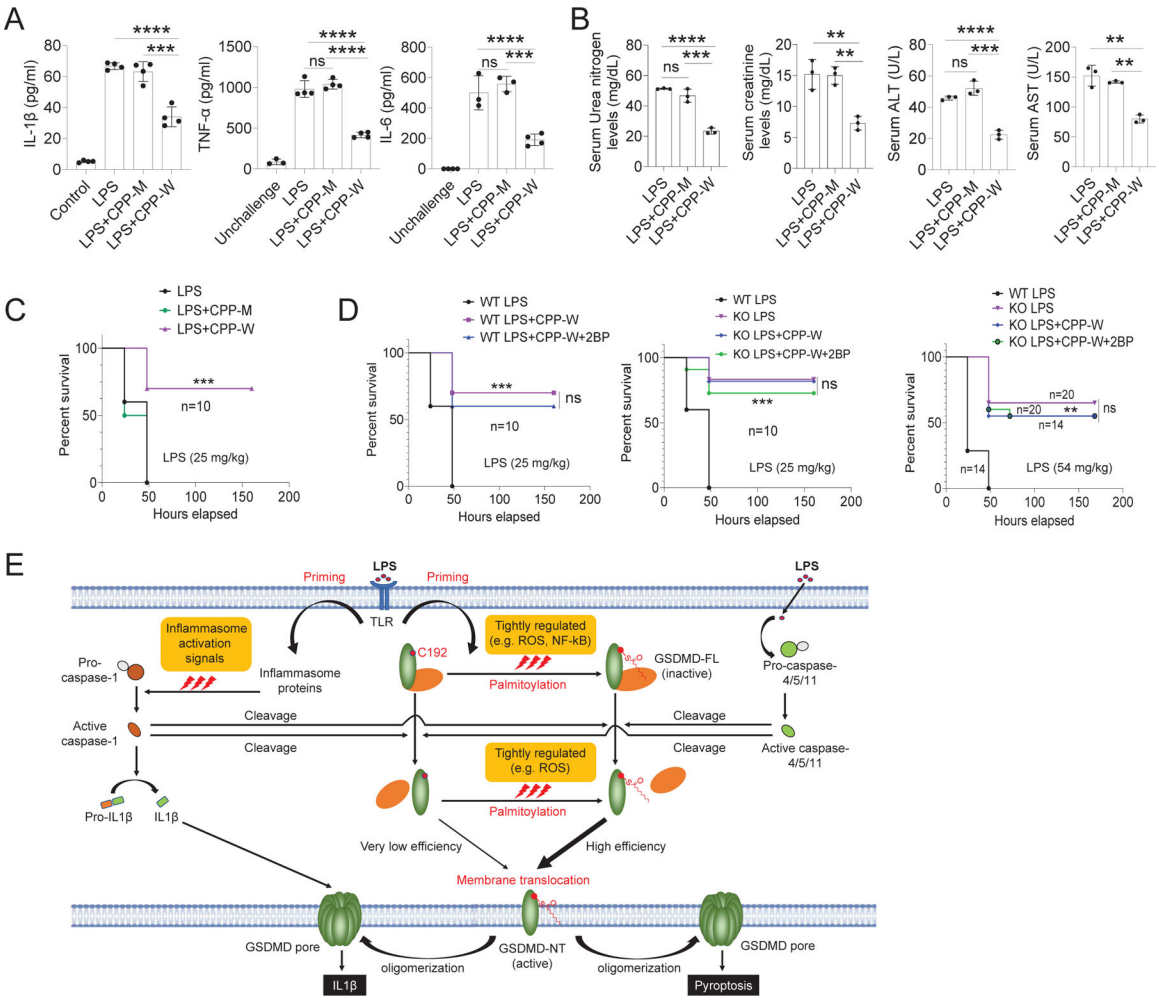

Fig. 7. Specific inhibition of GSDMD palmitoylation with CPP-W alleviates the severity of sepsis.

(**A**) Peritoneal fluid IL-1β, TNF-α, and IL-6 levels in sepsis induced by LPS (20 mg per kilogram of body weight) (n=3–4 mice per group). ***P<0.001, ****P<0.0001, one-way ANOVA followed by Bonferroni's multiple comparison test. (**B**) Circulating AST, ALT, BUN, and creatine levels in the serum. n=3 mice per group. **P<0.01, ***P<0.001, ****P<0.0001, one-way ANOVA followed by Bonferroni's multiple comparison test. (**C**) Survival rates were calculated using Kaplan–Meier survival curves. n=10 mice per group. The experiment was performed independently three times and the data were pooled and analyzed together. **P<0.01, ***P<0.001, log-rank (Mantel–Cox) test. (**D**) Survival rates were calculated using Kaplan–Meier survival curves. n=10–20 mice per group. The experiment was performed independently three times, and the data were pooled and analyzed together.**P<0.01, ***P<0.001, log-rank (Mantel–Cox) test. (**E**) Graphical illustration of GSDMD palmitoylation and its role in macrophage pyroptosis.